



**Michigan  
Technological  
University**

Michigan Technological University  
**Digital Commons @ Michigan Tech**

---

Michigan Tech Publications

---

3-12-2021

## Progress in proton-conducting oxides as electrolytes for low-temperature solid oxide fuel cells: From materials to devices

Wei Zhang

*Michigan Technological University, wzhang5@mtu.edu*

Yun Hang Hu

*Michigan Technological University, yunhangh@mtu.edu*

Follow this and additional works at: <https://digitalcommons.mtu.edu/michigantech-p>

 Part of the [Materials Science and Engineering Commons](#)


---

### Recommended Citation

Zhang, W., & Hu, Y. (2021). Progress in proton-conducting oxides as electrolytes for low-temperature solid oxide fuel cells: From materials to devices. *Energy Science and Engineering*. <http://doi.org/10.1002/ese3.886>

Retrieved from: <https://digitalcommons.mtu.edu/michigantech-p/14734>

Follow this and additional works at: <https://digitalcommons.mtu.edu/michigantech-p>

 Part of the [Materials Science and Engineering Commons](#)

## REVIEW

# Progress in proton-conducting oxides as electrolytes for low-temperature solid oxide fuel cells: From materials to devices

Wei Zhang | Yun Hang Hu 

Department of Materials Science and Engineering, Michigan Technological University, Houghton, MI, USA

**Correspondence**

Department of Materials Science and Engineering, Michigan Technological University, 1400 Townsend Drive, Houghton, MI 49931-1295, USA.  
Email: yunhangh@mtu.edu

**Funding information**

National Science Foundation, Grant/Award Number: CMMI-1661699

**Abstract**

Among various types of alternative energy devices, solid oxide fuel cells (SOFCs) operating at low temperatures (300–600°C) show the advantages for both stationary and mobile electricity production. Proton-conducting oxides as electrolyte materials play a critical role in the low-temperature SOFCs (LT-SOFCs). This review summarizes progress in proton-conducting solid oxide electrolytes for LT-SOFCs from materials to devices, with emphases on (1) strategies that have been proposed to tune the structures and properties of proton-conducting oxides and ceramics, (2) techniques that have been employed for improving the performance of the protonic ceramic-based SOFCs (known as PCFCs), and (3) challenges and opportunities in the development of proton-conducting electrolyte-based PCFCs.

**KEYWORDS**

energy devices, energy materials, proton conductors, protonic ceramic fuel cells

## 1 | INTRODUCTION

The extraordinary concerns regarding the depletion of fossil fuel resources and the emission of greenhouse gases have promoted considerable research activities on clean, sustainable, and highly efficient energy conversion and storage technologies. Fuel cells can directly convert the chemical energy in a fuel (eg, hydrogen and hydrocarbons) into electricity with high conversion efficiencies and low emissions. Based on types of electrolytes, fuel cells have been classified into alkaline fuel cell (AFC), proton exchange membrane fuel cell (PEMFC), phosphoric acid fuel cell (PAFC), molten carbonate fuel cell (MCFC), and solid oxide fuel cell (SOFC).<sup>1</sup>

AFCs, PEMFCs, and PAFCs, which are operated at low temperatures (<250°C), require pure hydrogen fuel to maintain stable performance, because hydrogen must be activated over noble metal catalysts (such as Pt) at low temperatures and these catalysts are easily poisoned by impurities (such as CO).<sup>2–4</sup> Therefore, hydrocarbons (such as natural gas) may not

be directly used for these fuel cells. In contrast, MCFCs and SOFCs are operated at high temperatures (650–1000°C).<sup>5,6a,6b</sup> Many catalysts are very active for hydrocarbons at high temperatures. Furthermore, catalysts have high tolerance for poisons at high temperatures.<sup>7,8</sup>

MCFCs use the molten salt of lithium potassium carbonate as an electrolyte at a high temperature, which can in situ convert fossil fuel to hydrogen-rich gases in the anode, eliminating the external production of hydrogen. However, carbonate electrolytes can easily corrode the anode and cathode, accelerating the degradation of MCFC components and decreasing the durability and cell life.<sup>9</sup> Therefore, in the area of high-temperature fuel cells, attention has been focused on SOFCs with metal oxide electrolytes.<sup>1,10</sup> The all-solid structure of SOFCs reduces the possibility of erosion, enabling the assembly of SOFC stacks/modules. Because SOFCs are made entirely of solid materials, they are not limited to the flat plane configuration and are also designed as rolled tubes.<sup>11</sup>

This is an open access article under the terms of the Creative Commons Attribution License, which permits use, distribution and reproduction in any medium, provided the original work is properly cited.

© 2021 The Authors. *Energy Science & Engineering* published by the Society of Chemical Industry and John Wiley & Sons Ltd.

The high operating temperature of SOFCs provides several advantages.<sup>6a,6b,7,12</sup> SOFCs can be run on a variety of fuels including natural gas. Noble metal catalysts (eg, Pt) are not required. Furthermore, waste heat from SOFC systems may be captured and reused, increasing the theoretical overall efficiency to as high as 70%-75%. Nevertheless, high operating temperatures also generate many challenges for SOFC systems.<sup>13-15</sup> One of them is the carbon dust deposited on the anode, which slows down the internal reforming process. It is also very difficult to well connect different components in SOFCs at high temperatures. Furthermore, high operating temperatures require the excellent thermal stability of materials, increasing the cost of the system. Therefore, decreasing the operating temperatures of SOFCs has become an important topic.<sup>16</sup>

It is well-known that the most common metal oxide electrolyte in SOFCs is a ceramic material called yttria-stabilized zirconia (YSZ), a typical oxide-ion conductor. YSZ and other oxide-ion conductors require a high temperature (750°C or above) to achieve desired ion conductivity.<sup>1</sup> In contrast, proton conductors exhibit higher ion conductivity at much lower temperatures (350-600°C) due to relatively low activation energy for proton migration in solid oxides.<sup>17</sup> Therefore, it is very attractive to develop SOFCs using a proton-conducting ceramic oxide as the electrolyte, which are also called as protonic ceramic fuel cells (PCFCs). However, only few reports show the peak power densities of PCFCs above 400 mW cm<sup>-2</sup> at 500°C,<sup>18-22</sup> which is a benchmark for traditional low-temperature SOFCs (LT-SOFCs).<sup>23-25</sup> Furthermore, some protonic ceramic electrolytes may react with CO<sub>2</sub>, challenging their utilization at a lower temperature with carbon-containing fuels.<sup>26</sup> This has stimulated intensive efforts to develop more efficient PCFCs, leading to the rapidly increased number of publications (Figure 1), particularly since 2000.

In recent years, several interesting review articles were published on the development of proton-conducting electrolytes for PCFCs.<sup>27-33</sup> However, each of them has focused on a specific material system or fabrication technique. Li et al reviewed the effects of sintering aids on the electrical conductivity of proton-conducting oxides without description about fuel cell (device) performances.<sup>33</sup> Kim et al summarized the applications of proton-conducting oxides in fuel cells, electrolysis cells, hydrogen purification, and ammonia synthesis with limited discussions about electrolyte materials.<sup>30</sup> So far, there has not been a comprehensive review to summarize recent advances in proton-conducting electrolytes and PCFCs at the level from materials to devices. This has encouraged us to write this review article: (1) Various types of proton conductors will be introduced, along with the principle and mechanism of proton conduction in crystal structures; (2) Strategies to tune the proton conductivity and chemical stability of proton-conducting oxides will be summarized,

followed by solutions of sinterability and electron leakage issues in proton ceramics; (3) Strategies of improving PCFC device performance from traditional methods to innovative concepts will be highlighted; (4) The challenges and opportunities in the development of proton-conducting electrolyte-based PCFCs will be discussed in the last section.

## 2 | TYPES OF PROTON CONDUCTORS

Proton conductors can be classified based on their working temperatures. Here, we summarize and discuss advances in high-temperature solid oxide proton conductors, which are generally employed as proton-conducting electrolytes in SOFCs. These materials are also known as high-temperature proton conductors (HTPCs) to distinguish them from proton-conducting polymer materials used in PEMFCs that operate at temperatures of <100°C.

### 2.1 | A<sup>2+</sup>B<sup>4+</sup>O<sub>3</sub>-type perovskite

The SrCeO<sub>3</sub>-based perovskite oxides were first found as the ABO<sub>3</sub>-type perovskite by Iwahara et al in 1981, showing proton conduction properties in hydrogen-containing atmosphere at 600-1000°C.<sup>34</sup> This stimulated great attempts to explore this type of perovskite, with the discovery of a series of proton conductors based on SrZrO<sub>3</sub>, BaCeO<sub>3</sub>, and CaZrO<sub>3</sub>, etc.<sup>35</sup> After nearly forty years of intensive research efforts, the perovskite-type cerates, and zirconates systems have been well-established.<sup>36-41</sup> The A-site cations are divalent (A<sup>2+</sup>, eg Ba<sup>2+</sup>, Ca<sup>2+</sup>, and Sr<sup>2+</sup>) and the B-site cations are quadrivalent (B<sup>4+</sup>, eg, Ce<sup>4+</sup> and Zr<sup>4+</sup>). Some trivalent dopants (eg, rare-earth elements) are usually employed to enhance the proton conductivity by introducing more oxygen vacancies, such as SrCe<sub>0.95</sub>Yb<sub>0.05</sub>O<sub>3-δ</sub>, SrZr<sub>0.95</sub>Y<sub>0.05</sub>O<sub>3-δ</sub>, BaCe<sub>0.9</sub>Y<sub>0.1</sub>O<sub>3-δ</sub>, BaCe<sub>0.9</sub>Nd<sub>0.1</sub>O<sub>3-δ</sub>, and CaZr<sub>0.9</sub>In<sub>0.1</sub>O<sub>3-δ</sub>.<sup>34,39,42-44</sup> They are generally written as AB<sub>1-x</sub>M<sub>x</sub>O<sub>3-δ</sub>, where M is the as-used

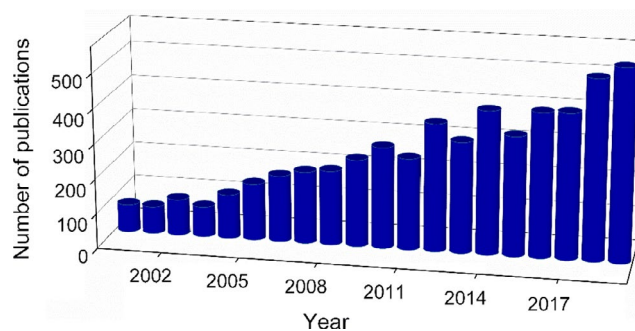
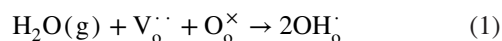


**FIGURE 1** Number of publications vs. publication years in the past two decades obtained from the Google Scholar database by searching for “protonic ceramic fuel cells”

dopants,  $\delta$  the number of oxygen vacancies per unit cell. A typical  $ABO_3$ -type perovskite crystal structure and possible proton conduction path in the crystal are shown in Figure 2.<sup>17</sup> Generally, protonic defects in these oxides are formed by the dissociative absorption of water at the surface, and the presence of oxide-ion vacancies is required. The absorbed water molecule dissociates into a hydroxide ion and a proton, then the hydroxide ion fills an oxide-ion vacancy ( $V_o^{\bullet}$ ), and the proton forms a covalent bond with the lattice oxygen ( $O_o^{\times}$ ). The process can be expressed as:



Electrical performance tests have been conducted on the doped cerates and zirconate-based proton conductors. The cerate-based perovskites show higher proton conductivity ( $10^{-2}$  to  $10^{-1}$  S  $cm^{-1}$  at  $600^\circ C$ ) than that of zirconate-based perovskites ( $\sim 10^{-3}$  S  $cm^{-1}$  at  $600^\circ C$ ).<sup>35</sup> However, chemical stability and mechanical strength of cerate-based ceramics are inferior to those of zirconate-based ceramics. This is because Zr-containing oxides react hardly with acid solution. Furthermore, they are very stable in  $CO_2$  atmosphere as well. In contrast, chemical reactions between the cerates and  $CO_2/H_2O$  gases can produce highly resistant carbonates/hydroxides, hindering their applications for SOFCs.<sup>45</sup>

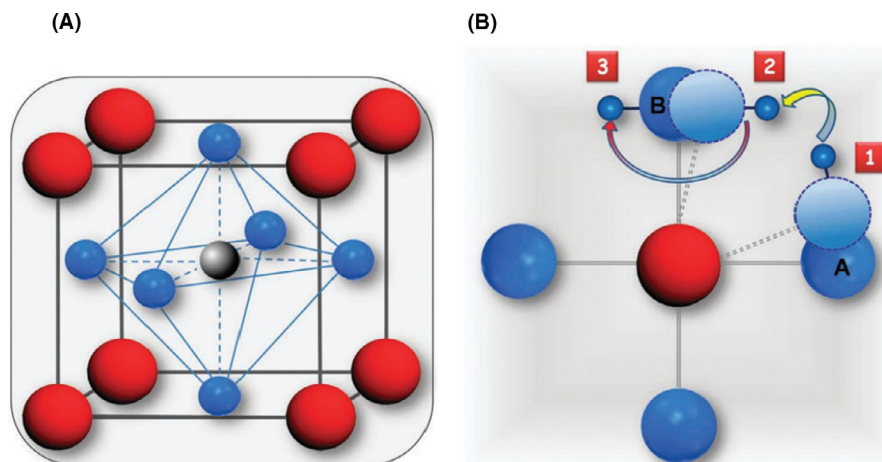
On the other hand, since cerates and zirconates are mutually soluble, the cerate-zirconate solid solutions have been intensively explored for the development of electrolytes with sufficient proton conductivity and decent chemical stability under fuel cell operating conditions.<sup>46–54</sup> For example, replacing a certain amount of Ce in the cerate by Zr is a well-recognized strategy that was proposed in 1999.<sup>55</sup> Among all known electrolyte materials,  $Ba(Zr_{0.1}Ce_{0.7}Y_{0.2})O_{3-\delta}$ , which was developed in 2006, displayed the highest ionic (protonic) conductivity, along with encouraging stability in  $CO_2$  and  $H_2O$  atmospheres.<sup>48</sup> Thus, the  $A^{2+}B^{4+}O_3$ -type perovskite (cerates and zirconates) has become one

of the most promising and active research areas in proton-conducting electrolytes. Currently, more attentions are being paid to co-doping strategies for optimizing their conductivity and stability, which will be further discussed in Section 3.

## 2.2 | $A^{3+}B^{3+}O_3$ -type perovskite

The  $A^{3+}B^{3+}O_3$ -type perovskite materials were also discovered as promising proton conductors, for example, doped  $LaYO_3$ ,  $LaErO_3$ , and  $LaScO_3$ .<sup>56–59</sup> Consequently, enhanced proton conductivity in Sr-doped perovskite  $La_{0.9}Sr_{0.1}MO_{3-\delta}$  ( $M = Sc^{3+}$ ,  $In^{3+}$ , and  $Lu^{3+}$ ) was reported by Nomura and coworkers.<sup>60</sup> The substitution of La by Sr in the perovskite is favorable for generating oxygen vacancies. The produced vacancies can trap water, and then, protons can be easily introduced into these oxides (as described by Equation 1). Among these materials, the compound with  $Sc^{3+}$  at the B site shows the highest proton conductivity of  $4 \times 10^{-3}$  S  $cm^{-1}$  due to the decreased size of the B-site cation from  $Lu^{3+}$  (0.861 Å) to  $Sc^{3+}$  (0.745 Å). In general, if the size of the B-site cation increases, oxygen sites would split gradually, and the dimensionality of proton conduction pathway would reduce from 3-D to 1-D, resulting in a decrease in proton concentration and mobility.<sup>61</sup> The conductivity could be further enhanced with more Sr-dopant ( $La_{0.8}Sr_{0.2}ScO_{3-\delta}$ ).<sup>62</sup> At  $600^\circ C$ , the compound with  $x = 0.2$  (ie, ratio of Sr to La) shows a proton conductivity of  $6 \times 10^{-3}$  S  $cm^{-1}$ , which is 1.5 times of that with  $x = 0.1$ . The proton conductivity of the optimized  $La_{0.8}Sr_{0.2}ScO_{3-\delta}$  material is significantly higher than that of  $A^{2+}B^{4+}O_3$ -type  $SrCe_{0.95}Yb_{0.05}O_{3-\delta}$  and very close to the value of  $BaCe_{0.95}Y_{0.05}O_{3-\delta}$  at the same temperature.<sup>63</sup> Moreover, the tolerance factor (0.91) of  $LaScO_3$  is higher than that (0.89) of  $A^{2+}B^{4+}O_3$ -type  $SrCeO_3$ , showing a higher structural stability. Therefore, the  $LaScO_3$ -type perovskite could be an alternative to cerate-based materials for the stable operation of SOFCs.

**FIGURE 2** (A) Typical  $ABO_3$ -type perovskite crystal structure, where red, gray, and blue spheres are an A-site cation, a B-site cation, and an oxide ion, respectively. (B) Proton conduction path from an oxide-ion A to another oxide-ion B in the perovskite crystal. Reprinted with permission from Ref. 17 Copyright 1972 Royal Society of Chemistry





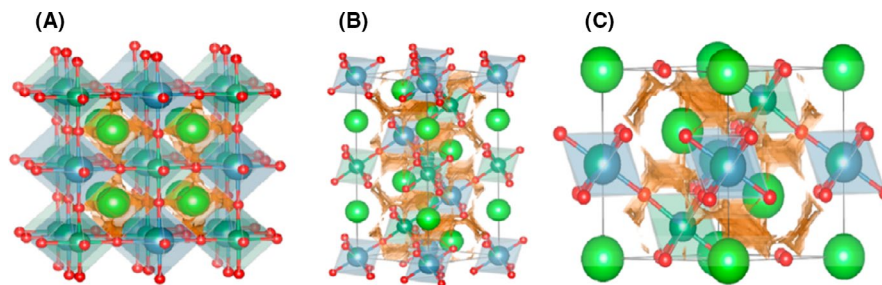


**FIGURE 3** Crystal structures of  $\text{Ba}_3\text{Ca}_{1+x}\text{Nb}_{2-x}\text{O}_{9.6}$  with (A)  $\text{Fm}\bar{3}\text{m}$ , (B)  $\text{R}\bar{3}\text{m}$ , and (C)  $\text{P}\bar{3}\text{m}1$  space groups. Ba, Ca, Nb, and O are light green, dark blue, dark green, and red spheres, respectively. The orange contour surfaces represent the low-energy pathway for protons in the bulk in (A)  $\text{Fm}\bar{3}\text{m}$ , (B)  $\text{R}\bar{3}\text{m}$ , and (C)  $\text{P}\bar{3}\text{m}1$  space groups. Reprinted with permission from Ref. 65 Copyright 2018 American Chemical Society

## 2.3 | Perovskite-related proton conductors

A wider class of perovskite oxides exists in the form of mixed perovskites. One of them is the  $\text{A}_2(\text{B}'\text{B}'')\text{O}_6$ -type perovskite, where the A ion is divalent, B' is trivalent, and B'' is pentavalent. The average charge on the B sites is 4+ when the compound is stoichiometric. Another type is the  $\text{A}_3(\text{B}'\text{B}'')\text{O}_9$ -type perovskite, where the B' ion is divalent, and A and B'' are still 2+ and 5+, respectively.<sup>64</sup> Notably, oxygen vacancies can be introduced in both of them by changing the stoichiometry, which means that the doping strategy is no longer necessary in these oxides.

Based on the above properties, one can increase the B'/B'' ratio to generate new oxides, for example,  $\text{A}_2(\text{B}'_{1+x}\text{B}''_{1-x})\text{O}_{6-\delta}$  and  $\text{A}_3(\text{B}'_{1+x}\text{B}''_{2-x})\text{O}_{9-\delta}$ . Nonstoichiometric mixed perovskites of  $\text{Sr}_2\text{Sc}_{1+x}\text{Nb}_{1-x}\text{O}_{6-\delta}$  ( $x = 0.05$  and  $0.1$ ) and  $\text{Ba}_3\text{Ca}_{1.18}\text{Nb}_{1.82}\text{O}_{9.6}$  are representative examples belonging to this class of complex perovskites, as studied by Nowick and coworkers.<sup>64</sup> Figure 3 gives the crystal structures of the  $\text{Ba}_3\text{Ca}_{1+x}\text{Nb}_{2-x}\text{O}_{9.6}$  based on different structural models ( $\text{Fm}\bar{3}\text{m}$ ,  $\text{R}\bar{3}\text{m}$ , and  $\text{P}\bar{3}\text{m}1$ ), showing the possible conduction pathway for protons.<sup>65</sup> These kind of materials were demonstrated to be good HTPCs on exposure to  $\text{H}_2\text{O}$ -containing atmospheres. The conductivities of them are expected to achieve the same range as those for doped  $\text{SrCeO}_3$  and  $\text{BaCeO}_3$ . Additionally, in contrast with cerate-based perovskites, these new structured materials do not show electronic conduction after treatment in highly reducing atmospheres and thus deserve more considerations as alternative electrolyte materials to the  $\text{ABO}_3$ -type perovskite for enhancing the electrochemical performance of fuel cell devices.

Some other materials are characterized by a disordered oxygen sublattice, in which the oxygen sites are only partially occupied. Typical representative of these perovskite-related oxides are  $\text{Sr}_{6-2x}\text{Nb}_{2+2x}\text{O}_{11+3x}$ ,  $\text{Sr}_{6-2x}\text{Ta}_{2+2x}\text{O}_{11+3x}$ , and  $(\text{Ba}_{1-y}\text{Ca}_y)_6\text{Nb}_2\text{O}_{11}$ .<sup>66,67</sup> They are able to incorporate up to one  $\text{H}_2\text{O}$  molecule per formula unit. More importantly, their conductivities are purely protonic at temperatures up to  $600^\circ\text{C}$ . However, the shortcoming of these materials is relatively low conductivity (less than  $10^{-3} \text{ S cm}^{-1}$ ), which is insufficient

for efficient fuel cells. Another perovskite-related proton-conducting material is  $\text{Ba}_2\text{In}_2\text{O}_5$ .<sup>68–72</sup> Its brownmillerite structure is derived from a perovskite-type crystal, where one sixth of the oxide ions are missing. However, its oxide-ion conductivity increases significantly when the temperature is higher than  $900^\circ\text{C}$ .<sup>73,74</sup> Sufficient proton conductivity may be obtained and stabilized under lower temperatures by partially replacing Ba and/or In, for example,  $\text{Ba}_2(\text{In}_{1-x}\text{Ti}_x)_2\text{O}_{5+x}$  and  $(\text{Ba}_{1-x}\text{La}_x)_2\text{In}_2\text{O}_{5+x}$  systems.<sup>75,76</sup> The further research on these perovskite-related systems will offer more opportunities for designing new proton conductors.

## 2.4 | Proton conductors with other crystal structures

Proton conduction has been observed in some materials without structural protons, for example,  $(\text{Li}/\text{Na}/\text{K})_3\text{PO}_4$  and other phosphate-based salts.<sup>77–79</sup> Because the larger  $\text{La}^{3+}$  ion is likely to be beneficial for proton mobility,  $\text{LaPO}_4$ -based materials are considered as potential proton-conducting electrolytes, which possess excellent ability to dissolve and transport protons with stable crystal structures. Furthermore, Norby and Christiansen observed decent proton conductivity in Ca- and Sr-substituted  $\text{LaPO}_4$ .<sup>80</sup> By introducing acceptor substituents with suitable ionic radii (eg, Ca and Sr), a high concentration of charge-compensating protons dissolved from water vapor was obtained. The proton conductivities are  $6 \times 10^{-5}$  and  $3 \times 10^{-4} \text{ S cm}^{-1}$  at  $800^\circ\text{C}$  for Ca- and Sr-substituted  $\text{LaPO}_4$ , respectively. These findings encourage further studies of proton conduction in phosphates. However, the doped  $\text{LaPO}_4$  has limited solubilities for dopant ions. Excess doping would lead to the formation of secondary phases and strong segregation. In addition to  $\text{LaPO}_4$ -based materials, other types of phosphates, for example, lanthanum polyphosphate ( $\text{LaP}_3\text{O}_9$ ) and lanthanum oxophosphate ( $\text{La}_7\text{P}_3\text{O}_{18}$ ) received more attentions.<sup>81,82</sup> Both of them have considerable proton conductivity in wet atmospheres, achieving  $\sim 3 \times 10^{-4} \text{ S cm}^{-1}$  at  $700^\circ\text{C}$  with Sr as the dopant, which is comparable to some perovskite-type materials like In-doped  $\text{CaZrO}_3$ .

Slater and coworkers demonstrated high-temperature proton conduction in a new phase of  $\text{La}_{1-x}\text{Ba}_{1+x}\text{GaO}_{4-x/2}$  that contains tetrahedral Ga, with significantly higher conductivity than that of other phases containing tetrahedral ions, for example, the doped  $\text{LaPO}_4$ .<sup>83</sup> Proton migration pathway around a  $\text{GaO}_4$  tetrahedron is shown in Figure 4, where the proton follows a curved path between two intratetrahedral oxide ions under repulsive interactions with adjacent cations.<sup>84</sup> Norby's group subsequently observed proton conduction in a series of acceptor-doped rare-earth ortho-niobates and ortho-tantalates, with a general formula of  $\text{RE}_{1-x}\text{A}_x\text{MO}_4$  ( $\text{RE} = \text{La, Nd, Gd, Tb, Er, or Y}$ ;  $\text{A} = \text{Ca, Sr, Ba}$ ;  $x = 0.01-0.05$ ;  $\text{M} = \text{Nb, Ta}$ ).<sup>85</sup> These materials have the mixed protonic, native ionic and electronic conduction properties depending on different conditions. The proton conductivity is dominant under humidified conditions below  $800^\circ\text{C}$ , and the highest proton conductivity of  $\sim 10^{-3} \text{ S cm}^{-1}$  was observed for Ca-doped  $\text{LaNbO}_4$ , showing potential as an electrolyte for PCFCs. More importantly, these materials possess relatively high proton conductivity among oxides that do not contain Ba or Sr, and thus, they are very suitable for fuel cells operating in  $\text{CO}_2$ -containing atmospheres. Notably, the major drawback of these materials is relatively low conductivity compared to perovskite-type cerate-based materials. Future efforts are necessary to solve the issue for practical PCFC applications.

### 3 | DEVELOPMENT STRATEGIES FOR PROTON-CONDUCTING ELECTROLYTES

#### 3.1 | Enhancement in proton conductivity

There are various compounds that exhibit remarkable proton conductivity, with an acceptor-dopant concentration of 10 mol% in most cases.<sup>86</sup> Using the  $\text{ABO}_3$ -type perovskite as an example, the level of conductivity is dependent on the nature of atoms in the perovskite: the conductivity generally increases with decreasing electronegativity of A and B elements. On the other hand, Kreuer showed that the formation enthalpy of proton defects decreases with decreasing electronegativity of elements, for example, from Ca to Ba (at A site) and from Ti to Ce (at B site).<sup>86</sup> According to these principles, the most developed proton-conducting systems are barium cerate ( $\text{BaCeO}_3$ ) and barium zirconate ( $\text{BaZrO}_3$ ) doped by divalent or trivalent elements.<sup>86</sup>

##### 3.1.1 | Single-doping strategy

It is possible to obtain sufficient defects in the sublattices of cerates and zirconates by a single doping. For example, by introducing an alkaline-earth element as dopant into the

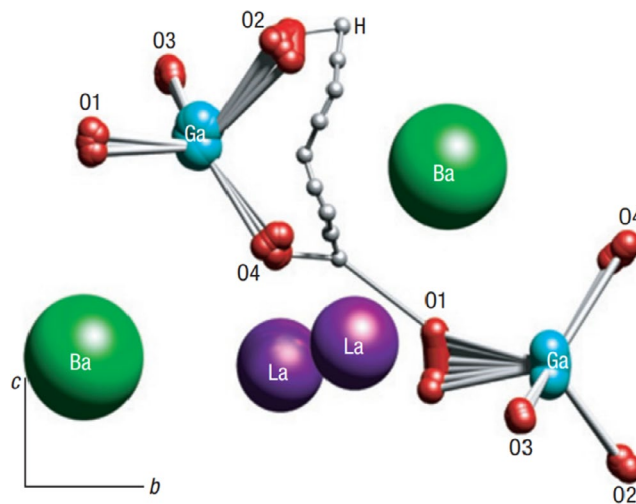
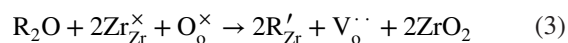
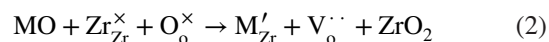


**FIGURE 4** Proton migration pathway around a  $\text{GaO}_4$  tetrahedron in the  $\text{La}_{1-x}\text{Ba}_{1+x}\text{GaO}_{4-x/2}$  crystal. The proton follows a curved path between two intratetrahedral oxide ions owing to repulsive interactions with adjacent large cations. Reprinted with permission from Ref. 84 Copyright 2007 Springer Nature

zirconate, the formation of oxygen vacancies can be represented by the Kröger–Vink notation<sup>87</sup>:



where M represents a divalent cation,  $\text{V}_\text{o}^{\cdot\cdot}$  a compensating oxygen vacancy, and R a trivalent cation. These equations indicate that the oxygen vacancies are formed by a compensating force of negatively charged defects.

All the elements of the lanthanide (Ln) series have been explored as dopant for the barium cerate: Pr, Nd, Sm, Eu, Gd, Tb, Dy, Ho, Er, Tm, Yb, and Lu.<sup>88–99</sup> The introduction of the Ln dopant can improve the conductivity of  $\text{BaCeO}_3$ -based materials. Namely, the conductivity of  $\text{BaCe}_{1-x}\text{Ln}_x\text{O}_{3-\delta}$  increases with increasing x, achieving the maximum at  $x = 0.1-0.25$ . This is a typical trend that has also been observed for other doped oxides.<sup>100</sup> However, the dissolution of  $\text{Ln}_2\text{O}_3$  into the perovskite structure forms free oxygen vacancies only at relatively low dopant concentrations, thus the decrease of conductivity with a further increased loading of  $\text{Ln}_2\text{O}_3$  is observed due to decreased oxygen vacancies.

The conductivity of  $\text{BaCe}_{0.9}\text{Ln}_{0.1}\text{O}_{3-\delta}$  ( $\text{Ln} = \text{La, Nd, Sm, Gd, Yb, Tb, or Y}$ ) is also dependent on structural parameters. It is generally accepted that lower distortion of the lattice and larger free volume can promote the ionic conductivity in perovskites. The degree of distortion is given by (and inversely proportional to) the Goldschmidt tolerance factor ( $t$ ):

$$t = \frac{r_A + r_O}{\sqrt{2}(r_B + r_O)} \quad (4)$$

where  $r_A$  and  $r_B$  are the ionic radii of cations located at A and B sites, respectively;  $r_O$  the ionic radius of oxygen. It was found that with increasing ionic radius of the dopant, the tolerance factor decreases.<sup>101</sup> On the other hand, the free volume, which is the difference between the volume of the unit cell and the volume of the constituent ions, increases with increasing ionic radius of the dopant. Thus, dopants with a smaller ionic radius generally exhibit a lower free volume and thus a decreased ionic mobility, whereas the smaller ionic radius tends to induce a larger tolerance factor and a higher ionic mobility. Therefore, Gd, Sm, and Y dopants, which possess the intermediate ionic radius (see Figure 5), are expected as the best candidates to optimize the ionic conductivity of barium cerates, as revealed by Amsif et al.<sup>101</sup> The Gd-doped  $\text{BaCe}_{0.9}\text{Gd}_{0.1}\text{O}_{3-\delta}$  exhibited the highest proton conductivity in the range of 200–900°C in wet 5%  $\text{H}_2$ -Ar, whereas the conductivity of Yb-doped  $\text{BaCe}_{0.9}\text{Yb}_{0.1}\text{O}_{3-\delta}$  and La-doped  $\text{BaCe}_{0.9}\text{La}_{0.1}\text{O}_{3-\delta}$  were lower than those of Sm, Y, and Gd-doped materials.

### 3.1.2 | Co-doping strategy

As an efficient strategy, simultaneous introduction of different types of ions at A and/or B sites is expected to optimize the electrical properties. Zhao et al partially doped  $\text{BaCeO}_3$  by both In and Y, leading to  $\text{BaCe}_{0.7}\text{In}_{0.3-x}\text{Y}_x\text{O}_{3-\delta}$  ( $0 \leq x \leq 0.3$ ), which exhibited an improved proton conductivity.<sup>102</sup> The fabricated fuel cells have a 45- $\mu\text{m}$  electrolyte by co-sintering electrolyte and anode at 1450°C. Using  $\text{BaCe}_{0.7}\text{In}_{0.1}\text{Y}_{0.2}\text{O}_{3-\delta}$  and  $\text{BaCe}_{0.7}\text{In}_{0.2}\text{Y}_{0.1}\text{O}_{3-\delta}$  as electrolytes, the power density reached 385  $\text{mW cm}^{-2}$  and 269  $\text{mW cm}^{-2}$  at 700°C, respectively. These values are comparable to the power density of a cell based on a thinner, single-doped  $\text{BaCe}_{0.7}\text{In}_{0.3}\text{O}_{3-\delta}$  electrolyte (20  $\mu\text{m}$ ).<sup>103</sup> This indicates the better proton conductivity of the In and Y co-doped electrolyte than the single-doped one. However, Zhang et al found that the proton conductivity of Ln (Y, Nd, Gd, and Yb) and In co-doped samples ( $\text{BaCe}_{0.8-x}\text{Ln}_{0.2}\text{In}_x\text{O}_{3-\delta}$ ) decreased with increasing In content.<sup>104</sup> This happened because the increase of In content decreases the lattice volume and proton concentration, hampering the proton diffusion.

The Y and Nd co-doped barium cerate at Ce site ( $\text{BaCe}_{0.8}\text{Y}_x\text{Nd}_{0.2-x}\text{O}_{3-\delta}$ ) was investigated by Su et al.<sup>105</sup> As x increases in  $\text{BaCe}_{0.8}\text{Y}_x\text{Nd}_{0.2-x}\text{O}_{3-\delta}$ , its conductivity increases to the maximum at  $x = 0.15$  and then decreases. Furthermore, Lee et al observed better phase stability of co-doped  $\text{BaCe}_{0.8}\text{Y}_x\text{Nd}_{0.2-x}\text{O}_{3-\delta}$  than that of single-doped  $\text{BaCe}_{0.8}\text{Y}_{0.2}\text{O}_{3-\delta}$ , but did not see the increase in conductivity with increasing x values.<sup>106</sup> This happened probably because the  $\text{BaCe}_{0.8}\text{Y}_x\text{Nd}_{0.2-x}\text{O}_{3-\delta}$  samples synthesized by these two groups possess different microstructures. Fu et al explored  $\text{BaCe}_{0.85}\text{Y}_{0.1}\text{Nd}_{0.05}\text{O}_{3-\delta}$  as an electrolyte for PCFCs.<sup>107</sup> A power density of 237  $\text{mW cm}^{-2}$  was obtained at 700°C based on a 50- $\mu\text{m}$  electrolyte with wet ethane fuel. Additionally,

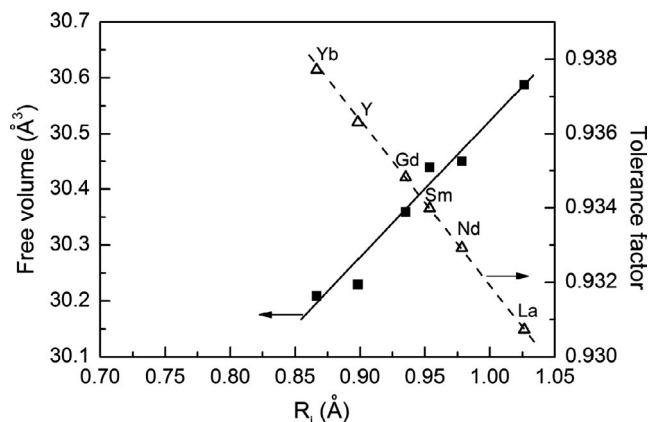


**FIGURE 5** Free volume and tolerance factor in various  $\text{BaCe}_{0.9}\text{Ln}_{0.1}\text{O}_{3-\delta}$  (Ln = La, Nd, Sm, Gd, Y, and Yb) samples as a function of ionic radius. Reprinted with permission from Ref. 101 Copyright 2011 Elsevier

Zhang and Zhao reported Sr and Nd co-doped  $\text{BaCeO}_3$  at both A and B sites ( $\text{Ba}_{1-x}\text{Sr}_x\text{Ce}_{0.9}\text{Nd}_{0.1}\text{O}_{3-\delta}$ ).<sup>108</sup> When Sr content increases from  $x = 0$  to  $x = 0.2$ , the structural distortion of the perovskite also increases, leading to a significant decrease in oxide-ion conductivity, but increasing the proton conductivity contribution to the total conductivity in both hydrogen-rich and oxygen-rich atmospheres. Therefore, Sr and Nd co-substituted  $\text{BaCeO}_3$  materials are considered as promising proton conductors for PCFCs if the composition can be further optimized.

### 3.2 | Increase in chemical stability

The application of  $\text{BaCeO}_3$ -based electrolytes in intermediate-temperature electrochemical devices is limited by poor stability in  $\text{CO}_2$  and water vapor atmospheres.<sup>109,110</sup> This promoted attempts to improve their stability. In this regard, the co-doping strategy plays a crucial role. Radojkovic' et al examined the structure change of Y and Nb co-doped  $\text{BaCeO}_3$ .<sup>111</sup> They prepared  $\text{BaCe}_{0.9-x}\text{Nb}_x\text{Y}_{0.1}\text{O}_{3-\delta}$  ( $x = 0-0.05$ ) materials by solid-state reaction method at 1000°C, generating a stable single-phase crystal at any Nb concentrations. Further sintering of the as-constructed ceramic tablet at 1550°C ensured a stable microstructure with a relative density of 92%–96%. The co-doped samples showed improved stability in pure  $\text{CO}_2$  at 700°C. However, the grain size of the samples decreased from 1.6 to 1.1  $\mu\text{m}$  as the Nb content increased, which caused the decrease of the conductivity from  $1.0 \times 10^{-2}$  to  $0.3 \times 10^{-2}$   $\text{S cm}^{-1}$  in wet hydrogen at 600°C. This is because more grain boundaries were produced, acting as a barrier of charges. In the sintered ceramics, both the grain interior and the grain boundaries contribute to the overall electrical performance. This means even though the grain interior is tuned to achieve enhanced proton conduction through the bulk, a high grain



boundary resistance may limit the practical use of the material. Increasing the sintering temperature is an effective strategy to obtain larger grains with fewer boundaries. However, the chemical composition of oxides could be changed under high-temperature conditions, as we discussed in section 3.3. Although a high Nb content negatively influences the conductivity, proton conduction is dominated rather than oxide-ion conduction because the enthalpy for vacancy hydration is less exothermal with the increasing Nb content.

The effects of Nb and Sm co-doping on the stability of BaCeO<sub>3</sub>-based ceramics were also explored. Xie et al synthesized BaCe<sub>0.8-x</sub>Nb<sub>x</sub>Sm<sub>0.2</sub>O<sub>3-δ</sub> system ( $x = 0-0.1$ ) by solid-state reaction method.<sup>112</sup> The adding of Nb into BaCe<sub>0.8</sub>Sm<sub>0.2</sub>O<sub>3-δ</sub> led to great stability in CO<sub>2</sub> and H<sub>2</sub>O-containing atmospheres, but decreased its conductivity due to the decline of free OH• vacancies. Similarly, Nb dopant can enhance the stability of BaCe<sub>0.8</sub>Gd<sub>0.2</sub>O<sub>3-δ</sub> in the presence of CO<sub>2</sub> and H<sub>2</sub>O, with a slightly lower conductivity as well.<sup>113</sup> The Sn and Y co-doped BaCe<sub>0.8-x</sub>Sn<sub>x</sub>Y<sub>0.2</sub>O<sub>3-δ</sub> ( $x = 0-0.25$ ) are very stable under fuel cell operating conditions and have acceptable proton conductivity in the temperature range of 600-1000°C.<sup>114</sup> More studies on the Sn-containing samples revealed that these materials can achieve higher relative densities of above 96% compared with single-doped BaCe<sub>0.8</sub>Y<sub>0.2</sub>O<sub>3-δ</sub> (88.3%).<sup>114</sup>

The chemical stability of barium cerate materials can also be improved by partial substitution of Ce with Ti, In, and Zr.<sup>115,116</sup> For example, Ti<sup>4+</sup> was doped into B site of BaCe<sub>0.8</sub>Y<sub>0.2</sub>O<sub>3-δ</sub> to modify its chemical stability.<sup>115</sup> Phase identification demonstrated that the resultant BaCe<sub>0.6</sub>Ti<sub>0.2</sub>Y<sub>0.2</sub>O<sub>3-δ</sub> remained the perovskite structure at a Ti-doping level of 20%. The exposure in 94% N<sub>2</sub> + 3% CO<sub>2</sub> + 3% H<sub>2</sub>O at 700°C for 10 hours did not change its structure. In contrast, significant decomposition was observed in single-doped BaCe<sub>0.8</sub>Y<sub>0.2</sub>O<sub>3-δ</sub>. The conductivity of the Ti-doped material reached  $7.2 \times 10^{-3}$  S cm<sup>-1</sup> at 700°C in wet H<sub>2</sub> condition, only slightly lower than the value of single-doped BaCe<sub>0.8</sub>Y<sub>0.2</sub>O<sub>3-δ</sub> ( $8.5 \times 10^{-3}$  S cm<sup>-1</sup>). Electrochemical performance of a fuel cell based on a 20-μm BaCe<sub>0.6</sub>Ti<sub>0.2</sub>Y<sub>0.2</sub>O<sub>3-δ</sub> electrolyte showed a peak power output of 244 mW cm<sup>-2</sup> at 700°C. Imperfectly, the open-circuit voltage (OCV) only reached 0.92 V, which is attributed to the partial reduction of Ce and Ti at the anode side, generating electronic defects. Besides, BaCe<sub>0.7</sub>A<sub>0.1</sub>Gd<sub>0.2</sub>O<sub>3-δ</sub> (A = In or Zr) system was also investigated.<sup>116</sup> All of the samples showed pure, stable perovskite structure. Particularly, the In-doped sample reached higher conductivity than the Zr-doped one in the range of 300-800°C because of better sintering densification.

### 3.3 | Improvement in sinterability

Improving the sinterability of proton-conducting ceramics is important for achieving high-performance electrolytes.

For example, the chemically stable yttrium-doped barium zirconate is refractory, which requires a very high sintering temperature (above 1700°C) and a long time to obtain both a single phase and a dense microstructure. Such a high temperature may accelerate the evaporation of barium from the oxide, leading to a decreased conductivity. It is also difficult to select ideal porous anode or cathode that can be combined with the refractory electrolyte for co-sintering at very high temperatures. For practical use, improvement of the sintering behavior of proton ceramics at reduced temperatures to maintain its high conductivity and chemical stability is critical. However, in a conventional solid-state reaction, solid precursors need to be fired at a high temperature (such as 1600°C) for more than 10 hours.<sup>117,118</sup> The required sintering temperature may be decreased using nanosized powders. Additionally, many sintering aids were successfully developed to improve the sinterability of proton ceramics.<sup>119-122</sup> However, some additives, for example, TiO<sub>2</sub>, MgO, MoO<sub>3</sub>, Al<sub>2</sub>O<sub>3</sub>, and Bi<sub>2</sub>O<sub>3</sub> have negative effects on the conductivity of the sintered ceramics.

Alternatively, dopants can affect the sinterability of proton-conducting ceramics. In general, it is difficult to achieve high conductivity, high sinterability, and excellent chemical stability simultaneously by using a single dopant. Using two or more dopants into the B site were found to be an effective strategy for improving the sintering properties and electrical performance of the perovskite-type proton ceramics.<sup>123-127</sup> For example, Liu and co-workers achieved the improvement in sinterability and proton conductivity for Sm and Y co-doped BaCeO<sub>3</sub>.<sup>128</sup> Doping BaZrO<sub>3</sub> with double dopants at the B site was also reported as an effective way to improve the sinterability.<sup>129</sup> Specifically, the performance of BaZr<sub>0.6</sub>M<sub>0.2</sub>Y<sub>0.2</sub>O<sub>3-δ</sub> with various M (M = Zr<sup>4+</sup>, Ce<sup>4+</sup>, Pr<sup>3+</sup>, Nd<sup>3+</sup>, Sm<sup>3+</sup>, and Gd<sup>3+</sup>) in addition to the Y-dopant were comparatively evaluated. The results show that (1) all the studied rare-earth dopants can improve the sinterability of materials; (2) the chemical stability of the compounds increases in CO<sub>2</sub> atmosphere with decreasing the ionic radii of M. Among various compositions, the Nd<sup>3+</sup> doped sample possesses the highest proton conductivity ( $8.56 \times 10^{-3}$  S cm<sup>-1</sup> at 600°C) along with excellent sinterability and resistance to CO<sub>2</sub>. Besides, the effects of dopants on the conductivity and sinterability of BaCe<sub>0.85</sub>Ln<sub>0.15</sub>O<sub>3-δ</sub> (Ln = Gd, Y, Yb) ceramics has been evaluated.<sup>130</sup> Y-doped sample shows the highest conductivity, while the sinterability depends on the ionic radius of the selected dopant. The obtained grain size of the ceramics decreases with decreasing ionic radius of the dopant. Furthermore, the sinterability and chemical stability of Y and In co-doped barium cerates (BaCe<sub>0.7</sub>In<sub>x</sub>Y<sub>0.3-x</sub>O<sub>3-δ</sub>) can be improved by increasing In concentration, but the electrical conductivity decreases.<sup>131</sup> This indicates that an intermediate composition is better for keeping a relatively high conductivity and an acceptable pellet density. More exploration of the

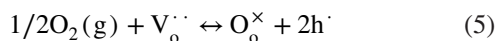


co-doping strategies is expected to achieve larger grain size and improve the relative density of the proton ceramics.

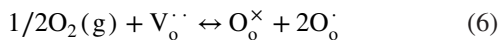
In summary, the following factors are generally beneficial to the proton conductivity of the sintered ceramics: (1) increase in the dopant concentration (eg, 10-20 mol% in most cases) of the oxide; (2) increase in the average grain size at optimized sintering temperatures; (3) increase in the relative density of the ceramic pellet; and (4) measurement atmospheres under highly reducing and humidified conditions. It is recognized that the sinterability is crucial to achieve the desired electrical performance among these factors. However, the conductivity can also be influenced by the synthesis route and synthesis temperature of the powders, as summarized in Table 1. This means that the conductivity is not always proportional to the relative density or grain size.<sup>132,133</sup>

### 3.4 | Minimization of electron leakage

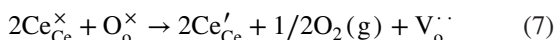
The electron leakage issue also deserves more attentions.  $\text{BaCe}_{0.2}\text{Zr}_{0.7}\text{Y}_{0.1}\text{O}_{3-\delta}$  is a well-developed solid solution as the proton ceramic system, but it is not a pure proton conductor. The material possesses four kinds of charge carriers: protonic defects ( $\text{OH}_o^\bullet$ ), oxygen vacancies ( $\text{V}_o^{\bullet\bullet}$ ), electrons ( $e^-$ ), and electron holes ( $h^\bullet$ ). The relative role of each carrier varies with local environment, for example, gas composition and temperature. After oxygen vacancies are generated (see Equations 2 and 3), proton ceramics is hydrated under humidified conditions as protons are incorporated into the lattice (Equation 1). However, this kind of hydrogen transport process via protonic defects is only the desired case in most applications. Under oxidizing conditions, electronic defects of holes are formed as oxygen species are incorporated into the lattice<sup>134–137</sup>:



These electronic defects are localized on the sites of lattice oxygen<sup>138–140</sup>:



Besides, under reducing atmospheres, significant electronic conduction in high Ce-containing samples can be observed,<sup>141</sup> where Ce ions are reduced to a lower oxidation state (ie,  $\text{Ce}^{3+}$ ) and thus electrons can be produced:



The generated electronic conductivity can significantly impair device performance, leading to reduced cell voltage and overall efficiencies.

From the perspective of energy efficiency, Nakamura and co-workers proposed that reducing the electrolyte thickness is not always an ideal approach to achieve high-performance PCFCs, since the energy loss becomes more significant in a thinner electrolyte due to internal current leakage.<sup>142</sup> Several strategies have been developed to mitigate the electron leakage in the electrolyte as much as possible. (1) Using an additional electron-blocking layer between the electrode and the electrolyte has been demonstrated as an effective way. For instance, a core-shell structured  $\text{Ce}_{0.8}\text{Sm}_{0.2}\text{O}_{2-\delta}$ (SDC)@ $\text{Ba}(\text{Ce}, \text{Zr})_{1-x}(\text{Sm}, \text{Y})_x\text{O}_{3-\delta}$  electron-blocking layer was in situ formed between Ni-BZY anode and SDC electrolyte.<sup>143</sup> The Ba-containing shell effectively protected SDC grains from reduction under fuel cell operating conditions, thus electronic conduction through the electrolyte was totally eliminated. However, this method may cause a larger interface resistance. (2) The double-layer electrolyte strategy can also be considered, as demonstrated in the bilayered BZCY/SDC structure for SOFCs with high OCVs.<sup>144</sup> These techniques of SOFCs are highly expected to be applicable for PCFC devices. (3) Tuning the composition of proton ceramics is another strategy. Dippon et al evaluated the effects of Ce content on the magnitude of electronic leakage in the  $\text{BaCe}_x\text{Zr}_{0.9-x}\text{Y}_{0.1}\text{O}_{3-\delta}$  electrolytes.<sup>145</sup> Minimized electron leakage was observed in samples with low Ce content. We can conclude that an intermediate composition is preferred for practical applications, where a negligible electronic conductivity and a relatively high protonic conductivity are achieved simultaneously.

## 4 | PROTON-CONDUCTING ELECTROLYTE-BASED PCFC DEVICES

SOFCs based on proton-conducting electrolytes are known as PCFCs. They have a sandwich structure (the same as conventional SOFCs), in which an anode and a cathode are separated by proton conductors (Figure 6).<sup>19</sup> PCFCs possess higher theoretical electromotive force and electrical efficiency compared with conventional oxide-ion-conducting SOFCs. Water is generated at the cathode instead of the anode, preventing fuel dilution at the anode and achieving efficient fuel managements. Furthermore, PCFCs have higher power output at low temperatures due to higher protonic conductivity, especially below 600°C. They are more suitable than oxide-ion SOFCs for lower operating temperatures.

Currently, the exploration of chemically stable proton conductors for PCFCs aims to achieve long-term, stable cell operation and reduce the costs of fuel cell systems. In addition, many novel strategies have been developed to achieve sufficient protonic conductivity and suppress the electronic conductivity in the electrolyte. Without doubt, the

**TABLE 1** Influence factors on proton conductivity. (Notes: BZY10: BaZr<sub>0.9</sub>Y<sub>0.1</sub>O<sub>3-δ</sub>; BZY20: BaZr<sub>0.8</sub>Y<sub>0.2</sub>O<sub>3-δ</sub>)

Electrolyte	Synthesis method	Synthesis temperature (°C)	Sintering temperature of pellet (°C)	Relative density (%)	Average grain size (μm)	Proton conductivity (mS cm <sup>-1</sup> )	Test temperature (°C)	Test atmosphere	Ref
BZY10	Solid-state reaction	n.a.	1500	98	1.3	2.1	700	Humidified H <sub>2</sub> or H <sub>2</sub> -inert gas mixture	218
BZY10	Solid-state reaction	n.a.	1600	97	2	1.9	700		219
BZY20	Sol-gel	1100	1600	80	n.a.	5.7	700		220
BZY20	Sol-gel	1000	1600	92.1	0.25	2.2	700		220
BZY20	Sol-gel	1000	1400	78.3	n.a.	10.4	600	Humidified inert gas	221
BZY20	Solid-state reaction	1200	1450	95	0.6	2.3	600		222
BZY20	Glycine-nitrate	1250	1600	99	0.46	8	600		223
BZY20	Citrate-nitrate	1200	1600	90	1	8.1	600		224
BZY20	Citrate-nitrate	1200	1600	90	0.44	5.6	600		224
BZY20	Co-precipitation	n.a.	1500	99.4	0.2	0.7	600		225

improvement of electrode performance is also important for proton-conducting electrolyte-based PCFCs.

#### 4.1 | Development of chemically stable electrolytes for PCFCs

The doped perovskite of SrCeO<sub>3</sub>-based oxide, which can conduct protons under hydrogen-containing atmosphere, was invented by Iwahara et al in 1981.<sup>34</sup> This stimulated great efforts to explore this type of proton conductors with the finding of SrZrO<sub>3</sub>, BaCeO<sub>3</sub>, BaZrO<sub>3</sub> systems, etc.<sup>35</sup> These materials were then widely studied as proton-conducting electrolytes for PCFCs.<sup>146–149</sup> Currently, the most developed proton-conducting electrolytes are based on BaCeO<sub>3</sub>, which have relatively large lattice free volume and relatively high geometrical symmetry, leading to the highest conductivities.<sup>150</sup> For practical applications in PCFC devices, the BaCeO<sub>3</sub>-based perovskites are usually substituted partially by Zr to achieve sufficient chemical stability, along with doping by different elements. (1) The Zr-containing perovskite BaZrO<sub>3</sub> is very stable under fuel cell operating conditions, which possesses similar proton conduction mechanism with BaCeO<sub>3</sub>, but with lower conductivity. The introduction of Zr into the BaCeO<sub>3</sub> achieved a balance between conductivity and chemical stability.<sup>55</sup> (2) Cations of rare-earth elements, such as Yb<sup>3+</sup>, Y<sup>3+</sup>, and Nd<sup>3+</sup>, were typically employed as dopants to introduce more oxygen vacancies into the perovskite structure. Table 2 shows the progress of PCFC device performances by employing the BaCeO<sub>3</sub>- and BaZrO<sub>3</sub>-based proton-conducting electrolytes in the recent decade.

Y-doped BaCeO<sub>3</sub> and BaZrO<sub>3</sub> (BCY and BZY) are two representative proton-conducting electrolytes at an early stage (Table 2). For example, Zunic et al employed electrophoretic deposition technique to prepare dense BCY electrolyte films on Ni-BCY composite anode substrates.<sup>151</sup> The deposition time was tuned to obtain a thickness of <15 μm, achieving a peak power density of 150 mW cm<sup>-2</sup> at 600°C (Figure 7A,B). Soon afterward, Bi et al developed an ionic diffusion strategy to prepare anode-supported BZY electrolyte films, leading to excellent chemical stability and improved performance (169 mW cm<sup>-2</sup> at 600°C) (Figure 7C,D).<sup>152</sup> Furthermore, BCY and BZY have been combined (BZCY) as a high performance, chemically stable electrolyte for PCFCs. Based on this electrolyte, Lee et al developed a gradient anode functional layer made of NiO and BZCY deposited on the BZCY electrolyte (Figure 8A), obtaining a power density of 240 mW cm<sup>-2</sup> at 600°C (Figure 8B).<sup>153</sup> Both the ohmic and polarization resistances were decreased due to the optimized microstructure of the anode functional layer on the BZCY electrolyte, which holds a continuously gradient interface to avoid the mismatch between electrolyte and anode. Fan and Su reported a triple-conducting (H<sup>+</sup>/O<sup>2-</sup>/e<sup>-</sup>), layer-structured

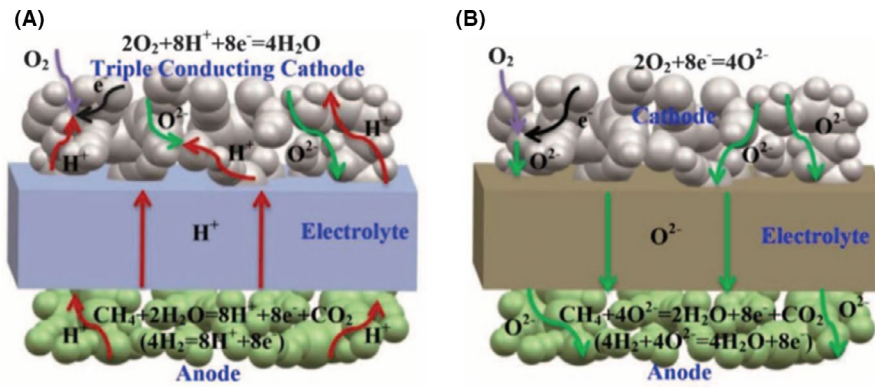


**FIGURE 6** Operation principles of a typical PCFC with a proton-conducting electrolyte (A) compared with an oxide-ion conducting SOFC (B). Reprinted with permission from Ref. 19 Copyright 2015 The American Association for the Advancement of Science

**TABLE 2** Electrochemical performances of PCFCs with BaCeO<sub>3</sub>-structured proton-conducting electrolytes

Electrolyte	Electrolyte thickness ( $\mu\text{m}$ )	Anode; cathode	OCV (V)	Power density ( $\text{mW cm}^{-2}$ )	Temp. ( $^{\circ}\text{C}$ )	Published year [Ref]
BCY10	13.4	Ni-BCY10; LSCF8282-BCYb10	0.98	150	600	2009 [151]
BCY10	85	Ni-BCY10; Pr2NiO4	1.145	96	600	2010 [226]
BZY20	4	Ni-BZY20; LSCF6428-BCYb10	0.99	110	600	2010 [227]
BZY20	20	Ni-BZCY172; SSC-SDC	1.014	70	600	2010 [228]
BZY20	20	Ni-BZY20; PBC-BZYP	0.97	169	600	2011 [152]
BZY20	25	Ni-BZCY172; SSC-SDC	0.97	55	600	2012 [229]
BZSY	12	Ni-BZSY; SSC-SDC	0.98	214	600	2013 [230]
BZCY35	20	Ni-BZCY35; SSC-BZCY35	1.04	240	600	2014 [153]
BZCYYb1711	14.7	Ni-BZCYYb1711; NBSCF	1.04	690	600	2014 [157]
BZCYYb1711	30	Ni-BZCYYb1711; BCFZY	1.1	650	600	2015 [19]
BZCY172	24	Ni-BZCY172; LNC-BZCY172	1.02	410	650	2016 [154]
BZCY172	20	Ni-BZCY172; SFNb	1.01	428	600	2017 [155]
BZCYYb1711	25	Ni-BZCYYb1711; LSCF6428-BZCYYb1711	1.08	331	600	2017 [231]
BZCY3	5	Ni-BZCY3; BSCF	1.056	1302	600	2018 [21]
BZCYYb4411	15	Ni-BZCYYb4411; PBSCF	1.01	1098	600	2018 [22]
BZCYYb1711	12	Ni-BZCYYb1711; LSCF6428-SDC	0.98	700	600	2019 [158]
BZCYYb1711	12	Ni-BZCYYb1711; LSM-SDC	0.95	580	600	2019 [159]

Note: All the cells were operated on humidified hydrogen and ambient air. (Notes: BCY10: BaCe<sub>0.9</sub>Y<sub>0.1</sub>O<sub>3-δ</sub>; LSCF8282: La<sub>0.8</sub>Sr<sub>0.2</sub>Co<sub>0.8</sub>Fe<sub>0.2</sub>O<sub>3-δ</sub>; BCYb10: BaCe<sub>0.9</sub>Yb<sub>0.1</sub>O<sub>3-δ</sub>; BZY20: BaZr<sub>0.8</sub>Y<sub>0.2</sub>O<sub>3-δ</sub>; LSCF6428: La<sub>0.6</sub>Sr<sub>0.4</sub>Co<sub>0.2</sub>Fe<sub>0.8</sub>O<sub>3-δ</sub>; BZCY172: BaZr<sub>0.1</sub>Ce<sub>0.7</sub>Y<sub>0.2</sub>O<sub>3-δ</sub>; SSC: Sm<sub>0.5</sub>Sr<sub>0.5</sub>CoO<sub>3-δ</sub>; SDC: Ce<sub>0.8</sub>Sm<sub>0.2</sub>O<sub>2-δ</sub>; PBC-BZYP: PrBaCo<sub>2</sub>O<sub>5+δ</sub>-BaZr<sub>0.7</sub>Y<sub>0.2</sub>Pr<sub>0.1</sub>O<sub>3-δ</sub>; BZSY: BaZr<sub>0.7</sub>Sn<sub>0.1</sub>Y<sub>0.2</sub>O<sub>3-δ</sub>; BZCY35: BaZr<sub>0.35</sub>Ce<sub>0.5</sub>Y<sub>0.15</sub>O<sub>3-δ</sub>; BZCYYb1711: BaZr<sub>0.1</sub>Ce<sub>0.7</sub>Y<sub>0.1</sub>Yb<sub>0.1</sub>O<sub>3-δ</sub>; NBSCF: NdBa<sub>0.5</sub>Sr<sub>0.5</sub>Co<sub>1.5</sub>Fe<sub>0.5</sub>O<sub>5+δ</sub>; BCFZY: BaCo<sub>0.4</sub>Fe<sub>0.4</sub>Zr<sub>0.1</sub>Y<sub>0.1</sub>O<sub>3-δ</sub>; LNC: LiNi<sub>0.8</sub>Co<sub>0.2</sub>O<sub>2-δ</sub>; SFNb: SrFe<sub>0.95</sub>Nb<sub>0.05</sub>O<sub>3-δ</sub>; BZCY3: BaZr<sub>0.3</sub>Ce<sub>0.55</sub>Y<sub>0.15</sub>O<sub>3-δ</sub>; BSCF: Ba<sub>0.5</sub>Sr<sub>0.5</sub>Co<sub>0.8</sub>Fe<sub>0.2</sub>O<sub>3-δ</sub>; BZCYYb4411: BaZr<sub>0.4</sub>Ce<sub>0.4</sub>Y<sub>0.1</sub>Yb<sub>0.1</sub>O<sub>3-δ</sub>; PBSCF: PrBa<sub>0.5</sub>Sr<sub>0.5</sub>Co<sub>1.5</sub>Fe<sub>0.5</sub>O<sub>5+δ</sub>; LSM: La<sub>0.75</sub>Sr<sub>0.25</sub>MnO<sub>3-δ</sub>).

LiNi<sub>0.8</sub>Co<sub>0.2</sub>O<sub>2-δ</sub> cathode for the BZCY-based PCFCs.<sup>154</sup> Simultaneous transport of intrinsic O<sup>2-</sup> and e<sup>-</sup> as well as extrinsic H<sup>+</sup> is illustrated in Figure 8C. The H<sub>2</sub>O-uptake capability of this material also facilitated the oxygen reduction reaction (ORR) process between the cathode and the BZCY electrolyte, leading to a power output of 410 mW cm<sup>-2</sup> at 650°C with the help of ZnO sintering aid (Figure 8D). Yuan et al reported a PCFC with the BZCY electrolyte and a Co-free cathode of SrFe<sub>0.95</sub>Nb<sub>0.05</sub>O<sub>3-δ</sub>, achieving a peak power density of 428 mW cm<sup>-2</sup> at 600°C with a low polarization

resistance (0.35 Ω cm<sup>2</sup>).<sup>155</sup> The fuel cell worked steady under a constant load of 140 mA cm<sup>-2</sup> at 550°C for 50 h without degradation.

The co-doping of Y and Yb created the renowned proton-conducting electrolyte BZCYYb, displaying an improved conductivity and excellent tolerance to S-poisoning and C-coking. This material has proton defects and oxide-ion vacancies, thus allowing fast transport of both ions (H<sup>+</sup> and O<sup>2-</sup>).<sup>156</sup> Kim et al evaluated the electrochemical performance of the BZCYYb electrolyte-based PCFCs with a perovskite

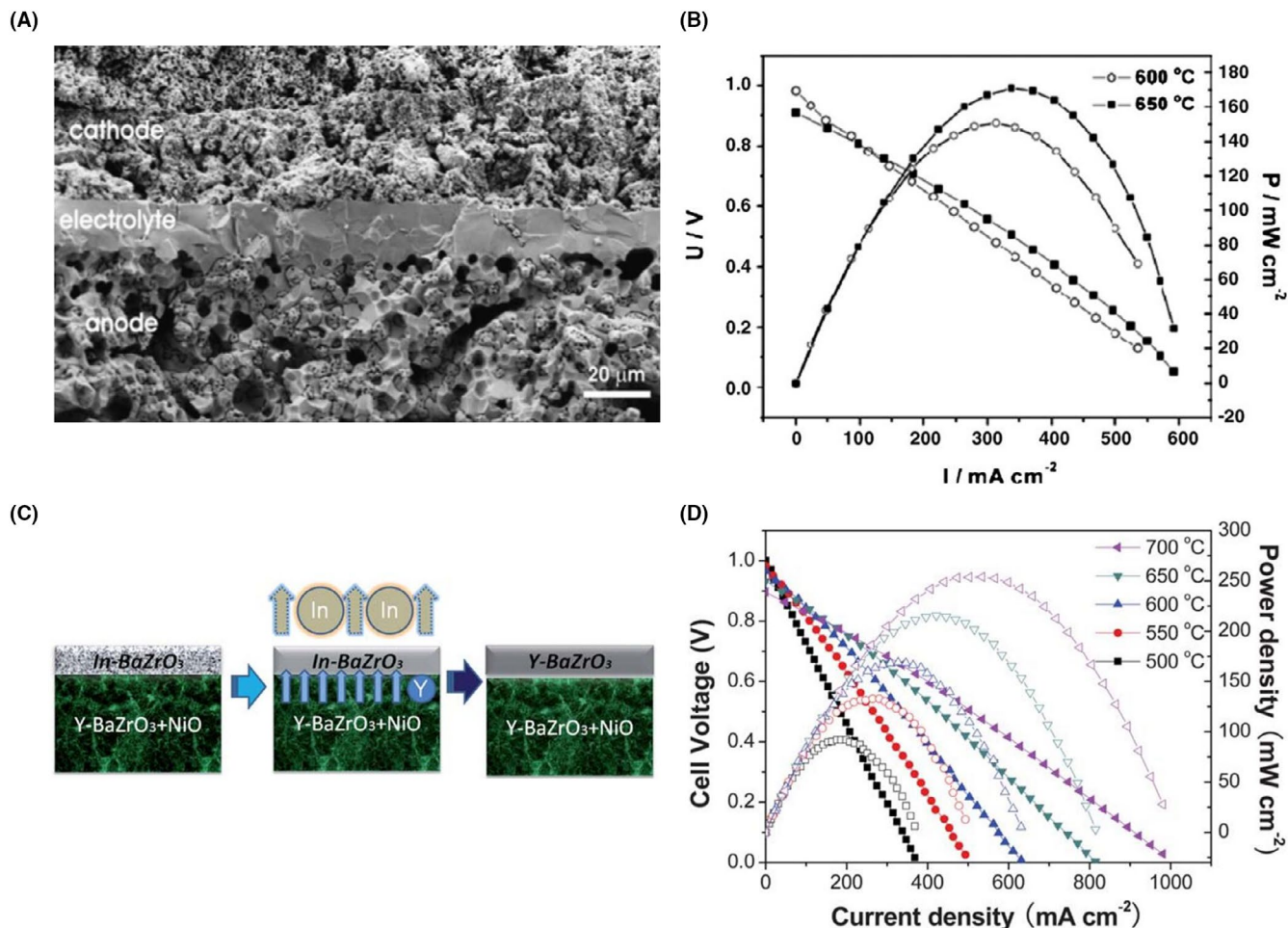


**FIGURE 7** Structure and performance of the PCFC with a dense BCY electrolyte prepared by electrophoretic deposition: (A) cross-sectional SEM image; (B) fuel cell performance. Reprinted with permission from Ref. 151 Copyright 2009 Elsevier. (C, D) Schematic diagram of preparing an anode-supported BZY electrolyte by ionic diffusion strategy and corresponding fuel cell performance. Reprinted with permission from Ref. 152 Copyright 2008 Royal Society of Chemistry

$\text{NdBa}_{0.5}\text{Sr}_{0.5}\text{Co}_{1.5}\text{Fe}_{0.5}\text{O}_{5+\delta}$  cathode and a Ni-BZCYYb anode.<sup>157</sup> The triple-conducting cathode extended the electrochemically active sites at the interface of the BZCYYb electrolyte and the cathode. The fuel cell showed long-term durability over 500 hours at 750°C with high-power densities of 1610  $\text{mW cm}^{-2}$  at 750°C and 690  $\text{mW cm}^{-2}$  at 600°C. Duan et al developed a triple-conducting cathode of  $\text{BaCo}_{0.4}\text{Fe}_{0.4}\text{Zr}_{0.1}\text{Y}_{0.1}\text{O}_{3-\delta}$  to improve the compatibility with the BZCYYb electrolyte.<sup>19</sup> The PCFC achieved a high-power density of 650  $\text{mW cm}^{-2}$  at 600°C and steady operation for 1100 hours under  $\text{H}_2/\text{air}$  conditions without degradation. Even when the operation temperature of the cell decreased to 350°C, it still reached a remarkable power density of  $\sim 100 \text{ mW cm}^{-2}$ . To reduce the interfacial resistance, Choi et al added a dense thin-film between the BZCYYb electrolyte and a porous  $\text{PrBa}_{0.5}\text{Sr}_{0.5}\text{Co}_{1.5}\text{Fe}_{0.5}\text{O}_{5+\delta}$  cathode (Figure 9B).<sup>22</sup> The dense thin-film possesses a sufficient solubility for  $\text{H}^+$  ions, which is beneficial to ORR at the oxidant/cathode interface. Consequently, the power density of

the PCFC was greatly enhanced to 1098  $\text{mW cm}^{-2}$  at 600°C (Figure 9D), with a long-term operation of 700 hours.

The refractory property of proton ceramic oxides is a major challenge. To solve this issue, An et al prepared a thin, dense BZCY electrolyte by anode-assisted densification, leading to a great breakthrough in PCFC performance and scalability.<sup>21</sup> With the help of a self-supplied transient phase from the anode (due to higher shrinkage of the anode), the BZCY electrolyte was uniformly densified on a Ni-BCZY anode at 1350°C (Figure 10A). This technique is useful to readily produce large-area PCFCs. The BZCY-based PCFC with a size of  $5 \times 5 \text{ cm}^2$  delivered an extremely high-power density of 1302  $\text{mW cm}^{-2}$  at 600°C (Figure 10B). Very recently, Chen et al developed a facile phase-coating strategy to fabricate a microtubular fuel cell based on the BZCYYb electrolyte.<sup>158,159</sup> Anode-substrate, electrolyte, and cathode were formed layer-by-layer on a glass rod using corresponding ceramic slurries followed by sintering (Figure 11A). With optimized coating times and sintering temperatures,



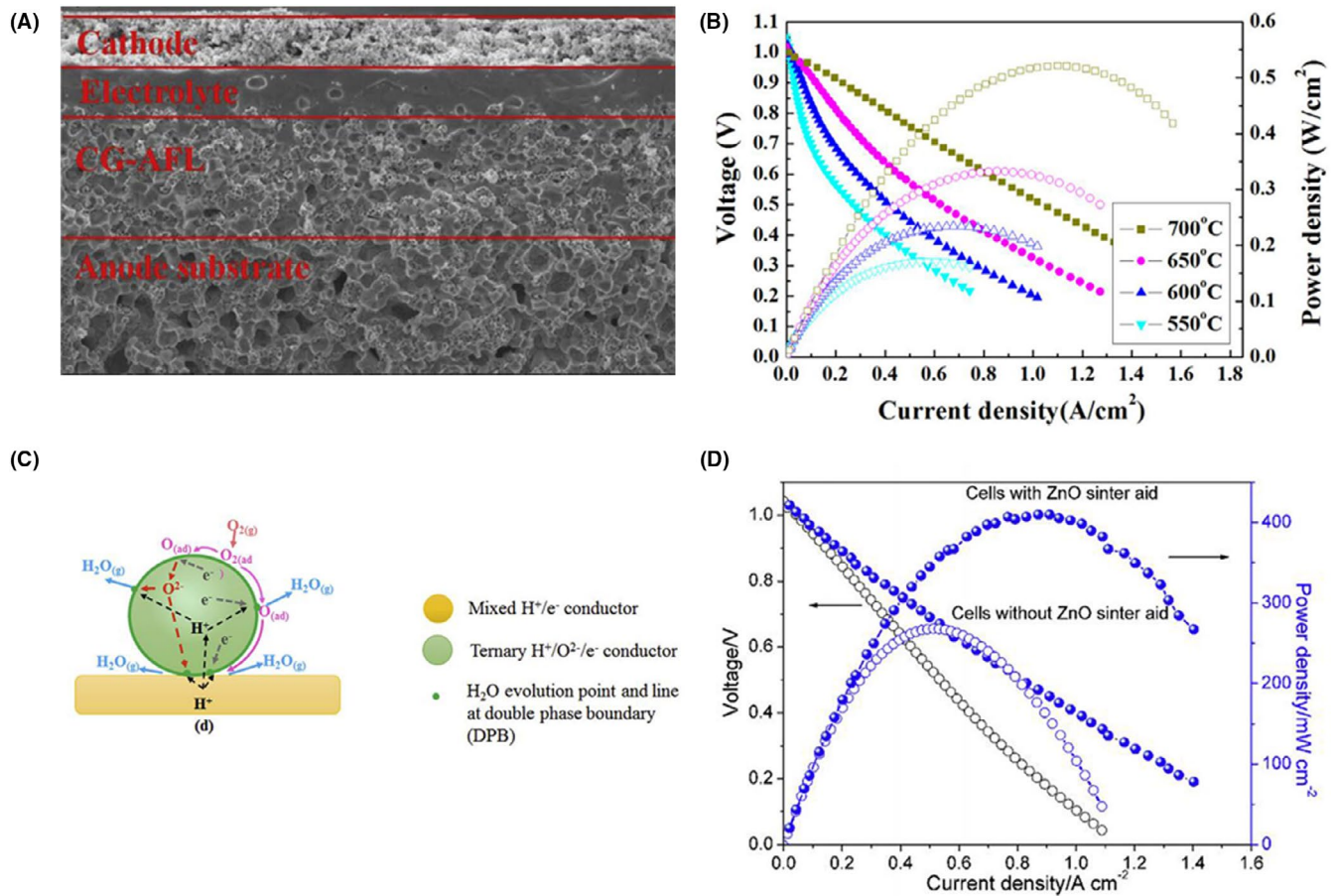


**FIGURE 8** (A, B) Cross-sectional SEM image and electrochemical performance of PCFC with the continuously gradient anode functional layer (CG-AFL). Reprinted with permission from Ref. 153 Copyright 2014 Elsevier. (C) Schematic diagram of simultaneous conduction of protons, oxide ions, and electrons in a triple-conducting cathode and (d) corresponding fuel cell performance. Reprinted with permission from Ref. 154 Copyright 2016 Elsevier

sponge-shaped anode and cathode were well-attached to the BZCYYb electrolyte. The large active areas of the electrode backbones lowered the polarization resistances and delivered a power density of  $700 \text{ mW cm}^{-2}$  at  $600^\circ\text{C}$  (Figure 11B). We believe these techniques are promising for mass production of commercial PCFCs.

## 4.2 | Novel semiconductor-based electrolytes for PCFCs

Semiconductor materials with proton-conducting properties could play an important role in future advanced PCFC technology. Recently, many semiconductor oxides have been explored as novel electrolytes for efficient fuel cells.<sup>160–167</sup> These new developments from traditional theory to innovative concepts have created a promising research frontier.

A fundamental challenge for the semiconductor electrolyte is the separation of electrons to prevent short circuiting.

Changing the oxidation states of transition elements may suppress the electronic conduction. Based on this principle, a new proton-conducting electrolyte was designed using a transition element-rich, layered-structured semiconductor  $\text{Li}_x\text{Al}_{0.5}\text{Co}_{0.5}\text{O}_2$ .<sup>168</sup> Under  $\text{H}_2/\text{air}$  operating conditions, this material experienced a significant transition, where the Co was reduced to divalent ions. Its electronic conduction was then eliminated due to the electron-insulating CoO bulk. Meanwhile, protons were readily incorporated into the interlayers of the semiconductor. The proton conductivity of this material achieved  $0.1 \text{ S cm}^{-1}$  at  $500^\circ\text{C}$ , with a power density of  $160 \text{ mW cm}^{-2}$  based on a thick ( $0.79 \text{ mm}$ ) electrolyte. Additionally, several semiconductor electrolyte systems (eg,  $\text{SrTiO}_3$ ,<sup>161</sup>  $\text{TiO}_2$ ,<sup>162</sup> and  $\text{BaCo}_{0.4}\text{Fe}_{0.4}\text{Zr}_{0.1}\text{Y}_{0.1}\text{O}_{3-\delta}$ -ZnO composite<sup>164</sup>) are based on an energy band alignment mechanism to eliminate electronic conductivity, providing new insight into the development of electrolytes. Namely, the energy band structure is carefully designed to tune (suppress) the transportation of electrons through the electrolyte in fuel cell devices, similar to some other semiconductor

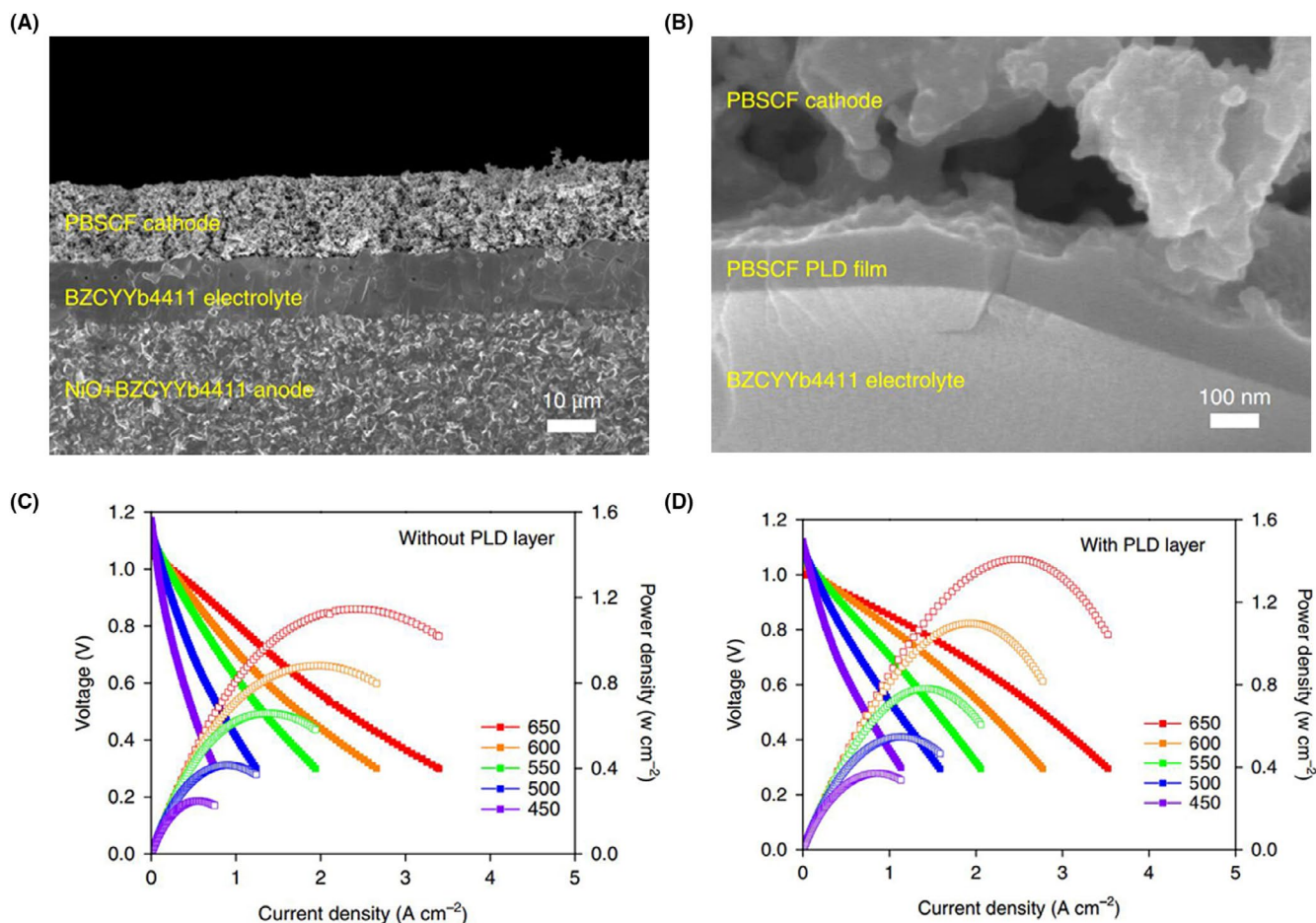


**FIGURE 9** Effect of interlayer on BZCYYb electrolyte-based PCFC: (A, B) Cross-sectional SEM image of the PCFC with a closer view showing the interlayer at the electrolyte/cathode interface; (C) fuel cell performance without the interlayer; and (D) with the interlayer. Reprinted with permission from Ref. 22 Copyright 2018 Springer Nature

devices, for example, solar cells. Typically, high OCVs of 1-1.1 V and power densities of 400-650  $\text{mW cm}^{-2}$  can be achieved at a relatively low temperature range of 500-550°C using these semiconductors as the electrolyte for fuel cells. Notably, almost pure proton conductivity was observed in a perovskite nickelate ( $\text{SmNiO}_3$ )<sup>160</sup> and a composite semiconductor of  $\text{Na}_x\text{CoO}_2\text{-CeO}_2$ .<sup>167</sup> Both of them have intrinsic electronic conductivity. However, in hydrogen-containing atmospheres, electronic conduction can be suppressed by a Mott transition that generates an electron-insulating layer in the  $\text{SmNiO}_3$  (Figure 12A,B) or by a local electric field generated with the semiconductor heterojunction in the composite  $\text{Na}_x\text{CoO}_2\text{-CeO}_2$  (Figure 12C,D). The latter case (composite) is more significant because the local electric field can simultaneously promote proton diffusion along the two-phase interface.<sup>169</sup> The composite semiconductor-based PCFC devices delivered a high-power density of 1000  $\text{mW cm}^{-2}$  at 520°C.<sup>167</sup>

Conventional solid-state ionics generally uses the doping strategy to design and create high-performance electrolytes.

However, fast ionic conduction can also be generated in non-doping semiconductors. Recently, a novel non-doping  $\text{CeO}_2$  has been designed as an electrolyte, with a  $\text{CeO}_{2-\delta}\text{@CeO}_2$  core-shell structure formed by surface hydrogenation.<sup>163</sup> It was found that this material exhibited high protonic conductivity.<sup>165</sup> High-concentration oxygen vacancies in the surface layer ( $\text{CeO}_{2-\delta}$ ) can promote proton conduction, creating continuous proton shuttles. The  $\text{CeO}_{2-\delta}\text{@CeO}_2$  electrolyte-based fuel cells have achieved  $\sim 700 \text{ mW cm}^{-2}$  at 520-550°C. Proton conduction in natural mineral is also promising. Electrolyte materials using delafossites,<sup>170</sup> hematites,<sup>171</sup> and mixed rare-earth carbonates<sup>172</sup> have shown their potential for developing cost-effective PCFCs. Power densities of 200-400  $\text{mW cm}^{-2}$  were achieved at  $\sim 550^\circ\text{C}$  by these mineral electrolyte-based fuel cells and could be further enhanced by their composites with other ionic materials. Proton transport through multi-phase interfaces (eg,  $\text{CuO}$ ,  $\text{Fe}_2\text{O}_3$ ,  $\text{SiO}_2$ , and  $\text{CaCO}_3$ ) is the main transport mechanism in these mineral oxides (Figure 13), which enables a low activation energy and rapid transport kinetics.<sup>171</sup>

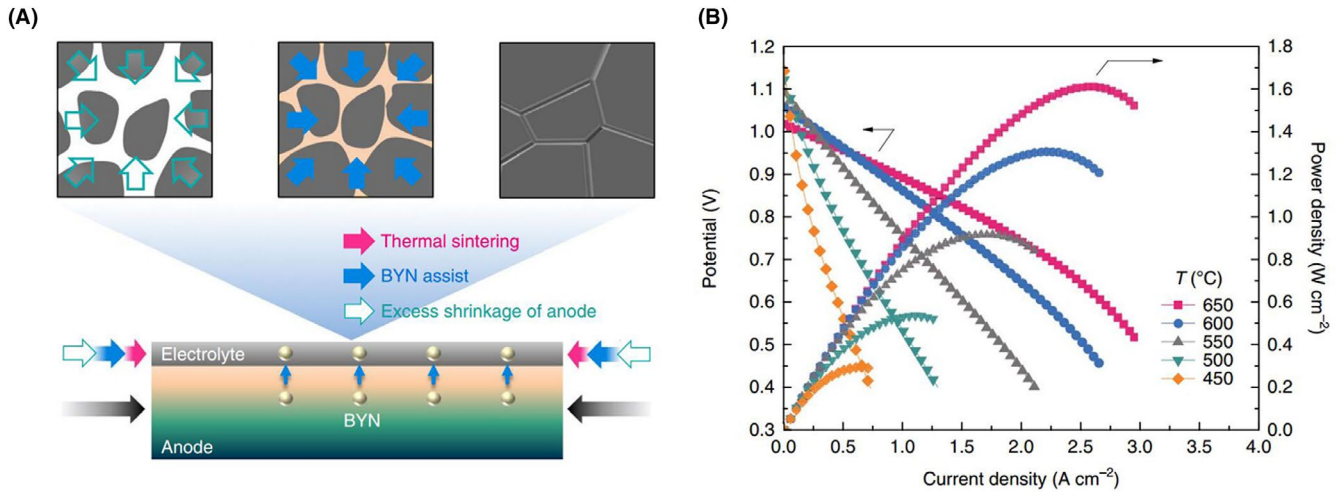


**FIGURE 10** (A) Schematic illustration of the BZCY electrolyte sintering processes driven by thermal sintering of the electrolyte (pink arrow), excess shrinkage of the anode (green arrow), and the assistance of  $\text{BaY}_2\text{NiO}_5$  from the anode (blue arrow); (B) corresponding cell performance. Reprinted with permission from Ref. 21 Copyright 2018 Springer Nature

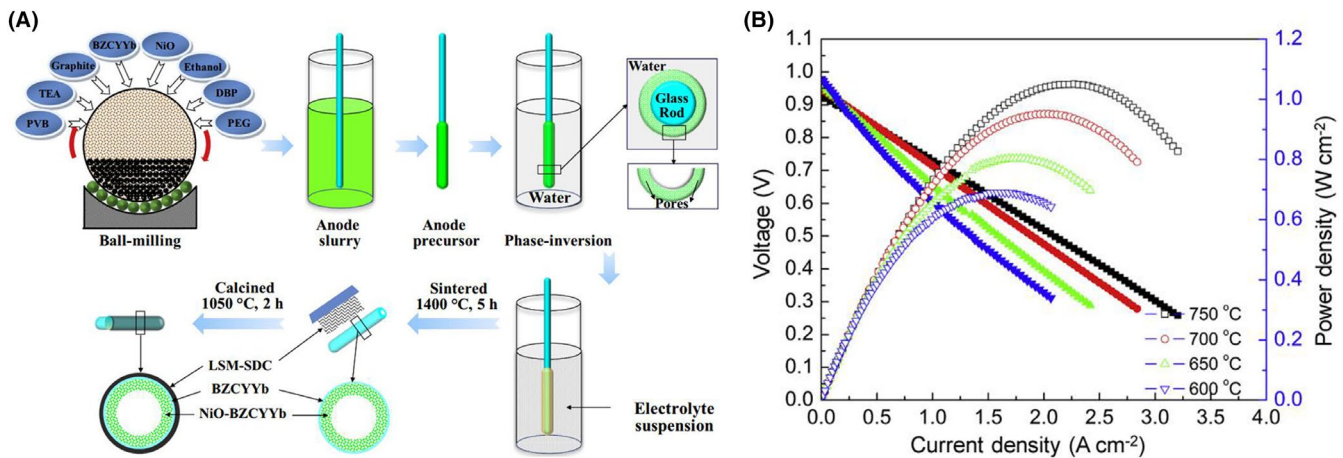


**FIGURE 11** (A) Flow chart of the phase-coating strategy for the fabrication of microtubular fuel cell based on BZCYYb electrolyte; (B) typical cell performance. Reprinted with permission from Ref. 158,159 Copyright 2019 Elsevier

## 4.3 | Improvement of electrode performance for PCFCs

### 4.3.1 | Cathode materials

Although PCFCs have shown great potential to be operated at lower temperatures than traditional SOFCs, their power output is still insufficient for practical applications, especially in the temperature range of 300-500°C. This is primarily limited by the lack of ideal cathodes that are compatible with proton-conducting electrolytes. As shown in Figure 14, ORR takes place at cathode, where  $\text{O}_2$  molecules are converted to  $\text{O}^{2-}$  ions by receiving electrons, which further combined with  $\text{H}^+$  to form water.<sup>157</sup> Cathode materials for PCFCs should possess high activity for ORR, allowing simultaneous transport of  $\text{H}^+$ ,  $\text{O}^{2-}$ , and  $e^-$  under fuel cell operating conditions, thus extending the active sites at the cathode/electrolyte

interface. Mixed ionic-electronic conductors (MIECs) were often selected as cathode for conventional SOFCs because of their excellent electronic conductivity and catalytic activity. However, MIECs are not suitable for PCFC cathode due to their poor proton conductivity, in which the electrochemically active sites are limited to the interface between the cathode and proton-conducting electrolyte (Figure 14).<sup>157</sup> Thus, the triple-conducting (ie,  $\text{H}^+$ ,  $\text{O}^{2-}$ , and  $e^-$ ) cathodes and the composite cathodes (eg, the mixture of MIECs and proton-conducting oxides) have been developed for PCFCs.

Doping is a useful strategy for developing electrochemically active triple-conducting cathode. Different alter-valent cations can be doped into a proton conductor (eg,  $\text{BaZrO}_3$  or  $\text{BaCeO}_3$ ) to enhance its electrochemical activity for oxide ions and electrons. For example, Mukundan et al doped Pr into the B site of  $\text{BaCe}_{0.8}\text{Gd}_{0.2}\text{O}_{3-\delta}$ , creating a triple-conducting cathode for barium cerate-based electrolytes.<sup>173</sup>



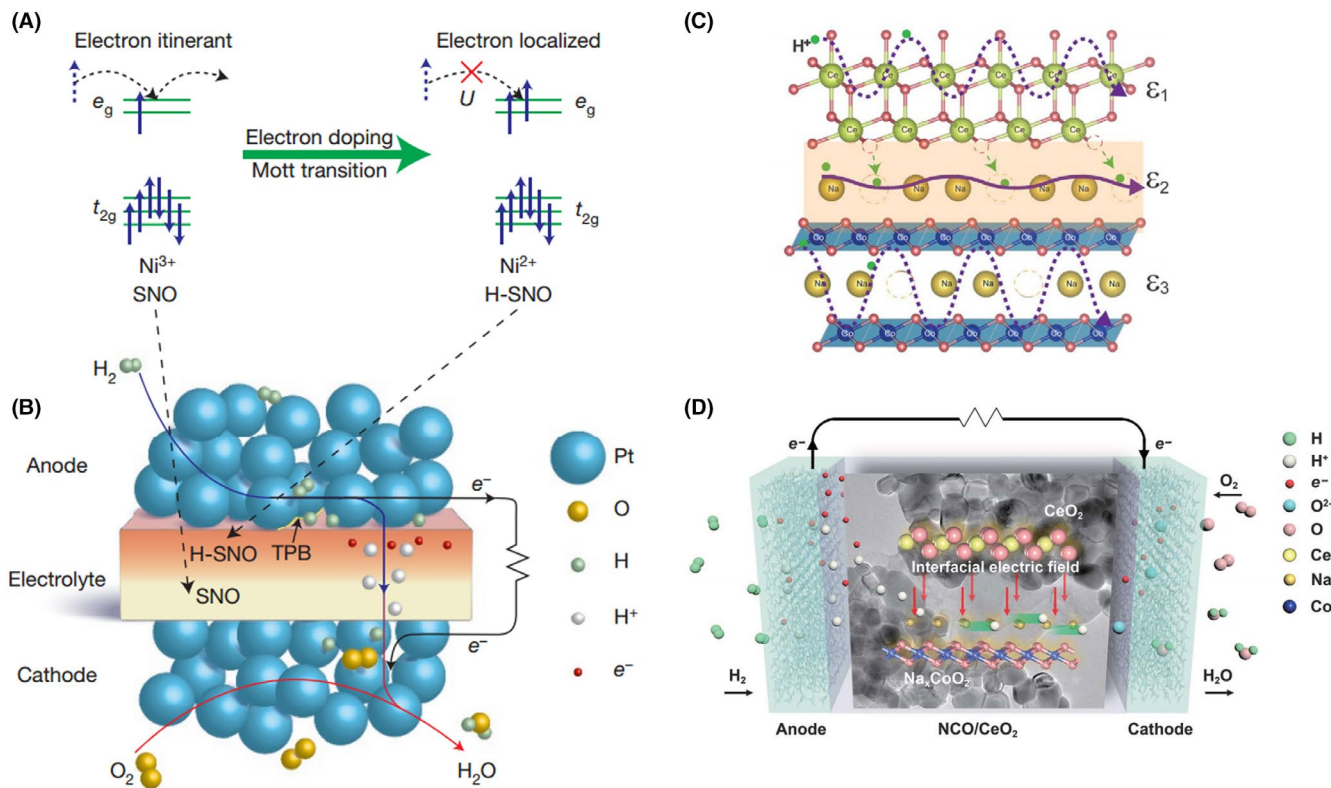


**FIGURE 12** (A) Mechanism of electron-blocking effect formed in the SmNiO<sub>3</sub> electrolyte; (B) Operation principle of the SmNiO<sub>3</sub> electrolyte-based fuel cell, where hydrogen incorporation creates an electron-insulating layer. Reprinted with permission from Ref. 160 Copyright 2016 Springer Nature. (C) Illustration of CeO<sub>2</sub> lattice, interfacial Na<sub>x</sub>CoO<sub>2</sub>-CeO<sub>2</sub> heterostructure, and Na<sub>x</sub>CoO<sub>2</sub> lattice. (D) Operation principle of the Na<sub>x</sub>CoO<sub>2</sub>-CeO<sub>2</sub> electrolyte-based fuel cell with a local electric field at the composite interface. Reprinted with permission from Ref. 167 Copyright 2020 The American Association for the Advancement of Science

However, this material showed insufficient protonic contribution with dominant p-type electronic conduction under oxidizing conditions. It possesses proton and oxide-ion conductivities, but its ionic transport numbers were decreased by the doping. Chemically stable BaZrO<sub>3</sub> doped by transition elements (eg, Co and Fe) has been demonstrated as an effective route for designing the triple-conducting cathode. In the BaCo<sub>0.4</sub>Fe<sub>0.4</sub>Zr<sub>0.2</sub>O<sub>3-δ</sub> (BCFZ) cathode, both proton and oxide-ion diffusions reduce the polarization resistance of the cathode, achieving significantly lower activation energy than the renowned La<sub>0.6</sub>Sr<sub>0.4</sub>Co<sub>0.2</sub>Fe<sub>0.8</sub>O<sub>3-δ</sub> (LSCF).<sup>174</sup> A power density of 225 mW cm<sup>-2</sup> was obtained at 600°C with the BZCYb electrolyte. Furthermore, Y-doped BaCo<sub>0.4</sub>Fe<sub>0.4</sub>Zr<sub>0.1</sub>Y<sub>0.1</sub>O<sub>3-δ</sub> (BCFZY) showed greatly improved ORR kinetics at low temperatures due to increased lattice parameter and free volume.<sup>175</sup> Under the same test conditions and cell configuration, the PCFC power density was improved to ~400 mW cm<sup>-2</sup> at 500°C with a stable operation for over 1000 hours. Very recently, Ren et al designed a novel A-site-deficient B<sub>x</sub>CFZY (Ba<sub>x</sub>Co<sub>0.4</sub>Fe<sub>0.4</sub>Zr<sub>0.1</sub>Y<sub>0.1</sub>O<sub>3-δ</sub>, x = 1, 0.95, 0.9) to promote the oxygen diffusion and hydration kinetics in the BCFZY material (Figure 15).<sup>176</sup> The as-designed Ba-deficiency introduced more oxygen vacancies

and protonic defects due to the charge compensation mechanism. The PCFC based on the Ba-deficient B<sub>x</sub>ZFCY cathode (Ni-BZCY/BZCY electrolyte/B<sub>0.9</sub>CFZY cathode) showed a power density of 376.27 mW cm<sup>-2</sup> at 500°C, demonstrating an effective strategy to tune the triple-conducting properties of perovskite materials.

Triple-conducting cathodes can also be derived from some MIECs by the absorption of water to obtain desired proton conductivity. Hydration and proton transport properties of the Pr<sub>2-x</sub>Sr<sub>x</sub>NiO<sub>4+δ</sub> were explored for PCFC cathodes.<sup>177</sup> The triple-conducting properties of Pr<sub>2</sub>NiO<sub>4+δ</sub> without Sr-doping (ie, x = 0) were clearly demonstrated under different pH<sub>2</sub>O conditions. The substitution of Pr<sup>3+</sup> by Sr<sup>2+</sup> in the Ruddlesden-Popper Pr<sub>2</sub>NiO<sub>4+δ</sub> could enhance its structural stability but with decreased protonic conduction. Large water uptake at high pH<sub>2</sub>O in Ba<sub>0.5</sub>Sr<sub>0.5</sub>Co<sub>0.8</sub>Fe<sub>0.2</sub>O<sub>3-δ</sub> (BSCF) and PrBaCo<sub>2</sub>O<sub>5+δ</sub> was also obtained, showing considerable proton conduction and therefore converting them to potential triple-conducting cathodes.<sup>178</sup> Other double-perovskite MIECs (eg, BaGd<sub>0.8</sub>La<sub>0.2</sub>Co<sub>2</sub>O<sub>6-δ</sub>, BaGdCo<sub>1.8</sub>Fe<sub>0.2</sub>O<sub>6-δ</sub>, and BaPrCo<sub>1.4</sub>Fe<sub>0.6</sub>O<sub>6-δ</sub>) were also explored as the cathode for PCFCs.<sup>179</sup> Furthermore, it was proposed that layered-structured perovskites not only provide pore channels for



oxide ions, but also exhibit better proton-conducting properties than other perovskite-related oxides due to their unique interlayers.<sup>178,180</sup> Some typical layered perovskite cathodes, for example,  $\text{NdBa}_{0.5}\text{Sr}_{0.5}\text{Co}_{1.5}\text{Fe}_{0.5}\text{O}_{5+\delta}$  (NBSCF) and  $\text{PrBa}_{0.5}\text{Sr}_{0.5}\text{Co}_{1.5}\text{Fe}_{0.5}\text{O}_{5+\delta}$  (PBSCF), have achieved power densities as high as 1000–1200  $\text{mW cm}^{-2}$  at 650°C with the BZCYYb electrolyte and Ni-BZCYYb anode operated under  $\text{H}_2/\text{air}$  conditions.<sup>22,157</sup> Notably, the lithiation of some transition metal oxides may introduce extrinsic proton conduction by forming a layered structure. Transition metal cations can be reduced to lower valence states in hydrogen-containing atmospheres, which allows the intercalation of protons in the lattice for charge compensation.<sup>168</sup> A lithiated transition metal oxide,  $\text{LiNi}_{0.8}\text{Co}_{0.2}\text{O}_2$ , showed higher ORR activity than most commonly used cathodes.<sup>154</sup> Extrinsic proton conduction originated from the layered structure was confirmed by water storage capability (hydration) of this oxide. Following this route, we believe that a series of triple-conducting cathode materials can be developed from cost-effective transition metal or alkaline-earth metal (eg, Ca, Cu, Fe, and Mn) oxides.

Composite cathodes can allow ones to extend the electrochemically active sites at the cathode/electrolyte interface for PCFCs. Typically, they can be formed by mixing

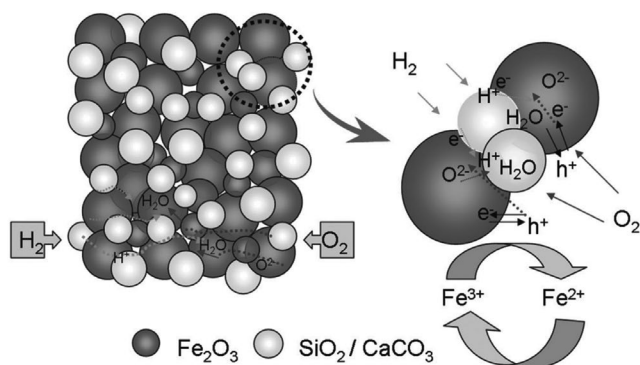


**FIGURE 13** Illustration of proton transport through multi-phase (eg,  $\text{Fe}_2\text{O}_3/\text{SiO}_2$  and  $\text{Fe}_2\text{O}_3/\text{CaCO}_3$ ) interfaces in the hematite mineral. Reprinted with permission from Ref. 171 Copyright 2015 John Wiley and Sons

a proton-conducting oxide and a MIEC material.<sup>181–183</sup> (1) Sufficient proton conductivity should be introduced into the MIECs; (2) Chemically stable composite cathodes under fuel cell operating conditions are required. Thus, proton conductors of barium cerates are not ideal candidates for the composite cathode, because the atmosphere at the cathode generally contains  $\text{CO}_2$  and  $\text{H}_2\text{O}$ . Zr-containing proton conductors can enhance the stability of the as-formed composite cathode with retaining decent proton conductivity. Progress in nanoparticle-embedded fibrous materials has been applied to manufacturing composite cathodes. For example, nanosized BZCY particles were embedded into the LSCF by electrospinning, forming a one-dimensional structured fibrous composite (Figure 16).<sup>184</sup> The porous and continuous structure is beneficial for mass transport and charge transfer in the cathode, leading to 239  $\text{mW cm}^{-2}$  at 550°C by a Ni-BCZY/BCZY/LSCF-BCZY cell configuration. Highly efficient composite cathodes can also be achieved by mixing MIECs with layered double-perovskite oxides, for example,  $\text{PrBaCo}_2\text{O}_{5+\delta}$  (PBC),  $\text{SmBaCo}_2\text{O}_{5+\delta}$  (SBC),  $\text{PrBaMn}_2\text{O}_{5+\delta}$  (PBM), PBSCF, and NBSCF due to their considerable proton-conducting properties.<sup>185–188</sup> For example, single-perovskite  $\text{Sm}_{0.5}\text{Sr}_{0.5}\text{CoO}_{3-\delta}$  (SSC) was combined with the layered SBC as a composite cathode for PCFCs, generating 1570  $\text{mW cm}^{-2}$  at 750°C using the BZCYYb electrolyte, with a low area specific resistance (ASR) of 0.021  $\Omega \text{ cm}^2$ .<sup>189</sup> High ORR activity can be achieved by the mixtures due to the triple-conducting properties of the layered perovskite, which improves the diffusivity of oxide ions and protons simultaneously. In addition, the operation stability of composite cathode-based PCFCs may be improved by controlling the porosity gradient in the cathode. For example, a gradient porous LSCF-BCZY cathode was developed for BCZY electrolyte-based fuel cells to accelerate the emission of water vapor from the cathode.<sup>190</sup> The porosity of the cathode was increased from ~24% (at the cathode/electrolyte interface) to ~38% (at the cathode surface) by electrostatic slurry spray deposition. Based on the gradient cathode, PCFC operated steady for 100 hours at a load of 175  $\text{mA cm}^{-2}$  at 600°C. A similar study using the  $\text{Sm}_{0.5}\text{Sr}_{0.5}\text{CoO}_{3-\delta}$  (SSC)

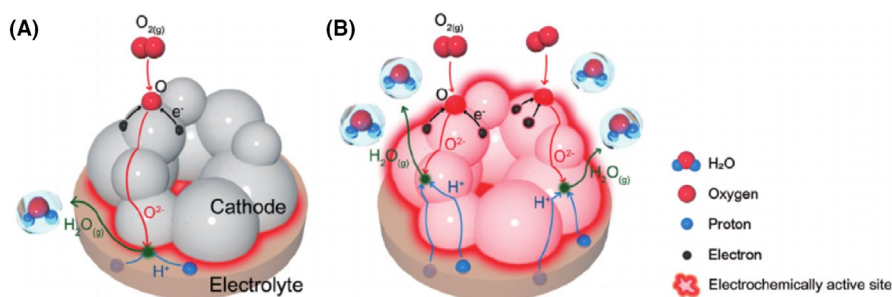


**FIGURE 14** Illustration of the ORR process at PCFC cathode using (A) MIEC ( $\text{O}^{2-}/\text{e}^-$ ) and (B) triple-conducting oxide ( $\text{H}^+/\text{O}^{2-}/\text{e}^-$ ) as the cathode material. The electrochemically active sites are greatly extended in the triple-conducting cathode. Reprinted with permission from Ref. 157 Copyright 2014 John Wiley and Sons

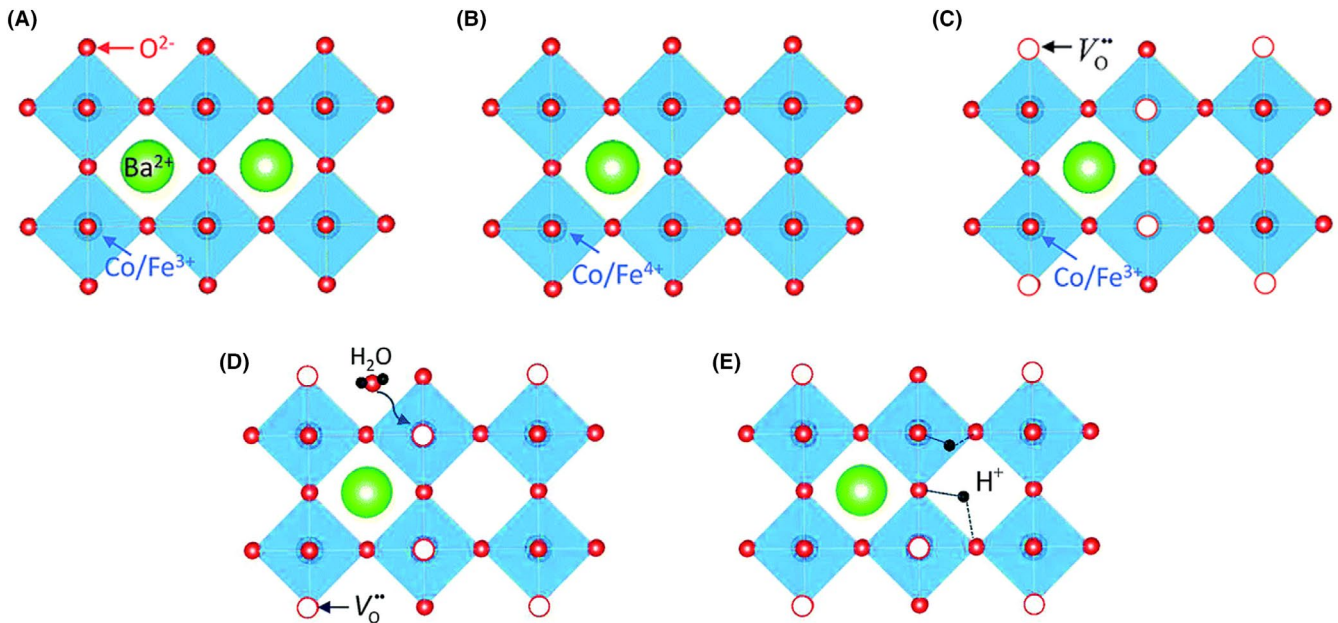
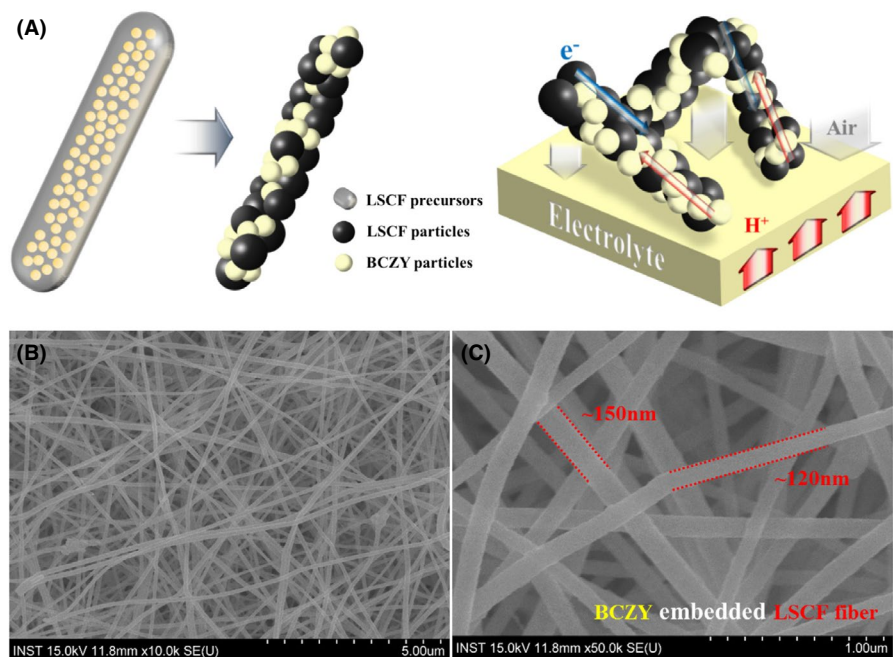


**FIGURE 15** (A-C) Illustration of the charge compensation mechanism in A-site-deficient  $B_xCFZY$  perovskites, showing the formation of Ba-deficiency and oxygen vacancies. (D, E) Illustration of the hydration reaction to form protonic defects. Reprinted with permission from Ref. 176 Copyright 2013 Royal Society of Chemistry

**FIGURE 16** (a) Schematic of the preparation of BCZY-embedded LSCF fiber and the as-formed LSCF-BCZY composite cathode on the electrolyte. (b, c) SEM images of LSCF fibers with embedded BCZY nanoparticles. Reprinted with permission from Ref. 184 Copyright 2018 Elsevier



to replace the LSCF achieved enhanced PCFC performances (over  $400 \text{ mW cm}^{-2}$  at  $700^\circ\text{C}$ ) because of enhanced surface diffusion of oxide ions.<sup>191</sup>

In situ exsolution is another promising method for the fabrication of high-performance composite cathodes. A composite cathode material based on the nominal composition of  $\text{La}_{0.5}\text{Ba}_{0.5}\text{CoO}_{3-\delta}$ - $\text{BaZrO}_3$  was prepared by exsolution of a single-phase  $\text{La}_{0.3}\text{Ba}_{0.7}\text{Zr}_{0.4}\text{Co}_{0.6}\text{O}_{3-\delta}$ , resulting in a  $\text{La}_{0.8}\text{Ba}_{0.2}\text{CoO}_{3-\delta}$  (40 mol%)- $\text{BaZr}_{0.6}\text{Co}_{0.4}\text{O}_{3-\delta}$

(60 mol%) composite, where the phase composition was tuned by thermal treatment.<sup>192</sup> The composite consists of larger  $\text{BaZr}_{0.6}\text{Co}_{0.4}\text{O}_{3-\delta}$  grains with the embedded, smaller  $\text{La}_{0.8}\text{Ba}_{0.2}\text{CoO}_{3-\delta}$  grains (Figure 17A,C), showing a high degree of contiguity between two phases, which is beneficial for fast proton conduction. In contrast, directly mixed (two-phase) sample without in situ exsolution shows almost the same grain size and a low degree of mixing (Figure 17B,D). The reported ASRs of this composite cathode are competitive

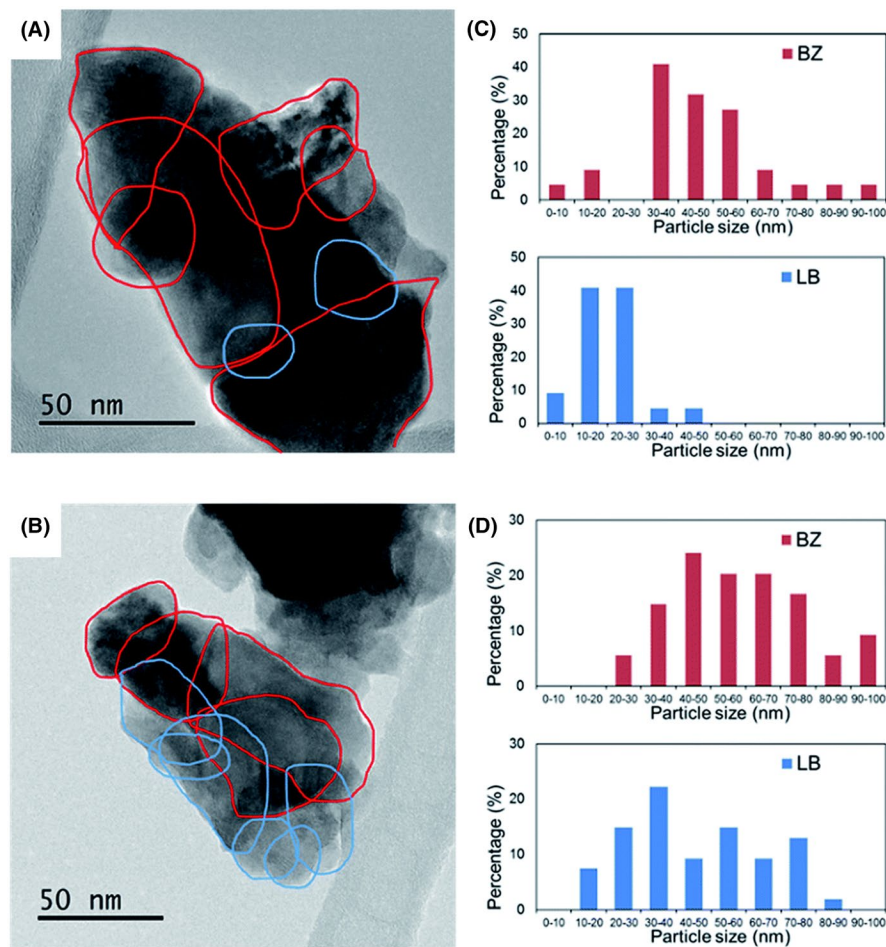


**FIGURE 17** TEM images of the composite cathode prepared by in situ exsolution (A) and directly mixing (B). The profiles of the  $\text{BaZr}_{0.6}\text{Co}_{0.4}\text{O}_{3-\delta}$  phase (BZ, red circles) and the  $\text{La}_{0.8}\text{Ba}_{0.2}\text{CoO}_{3-\delta}$  phase (LB, blue circles) are plotted. Grain size distribution of the exsolved sample (C) and the mixed sample (D). Reprinted with permission from Ref. 192 Copyright 2013 Royal Society of Chemistry

(namely,  $1.54 \Omega \text{ cm}^2$  at  $600^\circ\text{C}$  and  $18 \Omega \text{ cm}^2$  at  $400^\circ\text{C}$ ), with low activation energy of  $\sim 60 \text{ kJ mol}^{-1}$ . The infiltration method is also effective for tuning the cathode performance. Duan et al infiltrated BCFZY nanoparticles into a porous BZCY skeleton as a composite cathode, achieving a high porosity with excellent proton conductivity.<sup>175</sup> Compared with other single-phase BZFCY cathodes, the highest PCFC power density ( $455 \text{ mW cm}^{-2}$  at  $500^\circ\text{C}$ ) was obtained with this composite cathode under  $\text{H}_2/\text{air}$  atmosphere. Similarly, Li et al prepared a  $(\text{Pr}_{0.9}\text{La}_{0.1})_2(\text{Ni}_{0.74}\text{Cu}_{0.21}\text{Nb}_{0.05})\text{O}_{4+\delta}$ -infiltrated BZCY composite cathode.<sup>193</sup> The Nb-doped catalyst aims to increase the concentration of interstitial oxygen and enhance the structural stability. The resulting composite facilitates oxygen surface exchange and overall cathode reaction. Very recently, a nanoscaled self-assembly technique was explored for the preparation of triple-conducting composite cathodes to address the issues of inhomogeneity between different phases.<sup>194</sup> Namely, a nominal single-phase composition of  $\text{BaCo}_{0.7}(\text{Ce}_{0.8}\text{Y}_{0.2})_{0.3}\text{O}_{3-\delta}$  was self-assembled into several phases during calcination and fuel cell operating, where the new phases are homogeneous and closely contacted with each other (Figure 18B). Different functionalities were achieved by the as-produced three phases, namely,  $\text{BaCe}_x\text{Y}_y\text{Co}_z\text{O}_{3-\delta}$  ( $\text{H}^+/\text{e}^-$  conducting),  $\text{BaCo}_x\text{Ce}_y\text{Y}_z\text{O}_{3-\delta}$  ( $\text{O}^{2-}/$

$\text{e}^-$  conducting), and  $\text{BaCoO}_{3-\delta}$  ( $\text{e}^-$  conducting). Based on this composite cathode, high-power densities (eg,  $\sim 1000 \text{ mW cm}^{-2}$  at  $650^\circ\text{C}$ , Figure 18C) were obtained, while a robust operational stability was maintained for more than 800 hours at  $550^\circ\text{C}$  (Figure 18D).

There are some other issues regarding the chemical and thermal compatibility of PCFC cathodes. During the co-sintering on the electrolyte surface, the diffusion of cations between cathode and electrolyte may form an interfacial phase, which is detrimental to the long-term operation of PCFCs. For example, several compounds, such as  $\text{La}_{0.1}\text{Sr}_{0.1}\text{Ce}_{0.8}\text{O}_{2-\delta}$  and  $\text{La}_{0.4}\text{Ce}_{0.6}\text{O}_{2-\delta}$ , were formed between  $\text{LaMO}_3$  ( $\text{M} = \text{Mn}, \text{Fe}, \text{Co}$ ) cathode and proton conductor  $\text{SrCeO}_3$  during long-term heat treatment at  $1150^\circ\text{C}$ .<sup>195</sup> The dissolution of  $\text{SrO}$  from  $\text{SrCeO}_3$  into  $\text{LaMO}_3$  produced these interfacial phases, which is driven by the high activity of  $\text{SrO}$ . To suppress the formation of impurity phases, the Ruddlesden–Popper structured cathodes (eg,  $\text{La}_2\text{NiO}_4$ ) have been identified as better candidates for  $\text{SrCeO}_3$ -based electrolytes, where the interfacial reaction is less pronounced.<sup>195</sup> On the other hand, the interfacial reaction may enhance the electronic conductivity in some cathodes. Goupil et al studied the compatibility between the proton conductor  $\text{BaZr}_{0.9}\text{Y}_{0.1}\text{O}_{3-\delta}$  and a series of cathodes,  $\text{MCoO}_3$  ( $\text{M} = \text{La}, \text{Sr}, \text{Ba}$ ),  $\text{Ba}_{0.5}\text{La}_{0.5}\text{CoO}_{3-\delta}$ ,  $\text{Sr}_{0.5}\text{La}_{0.5}\text{CoO}_{3-\delta}$ ,



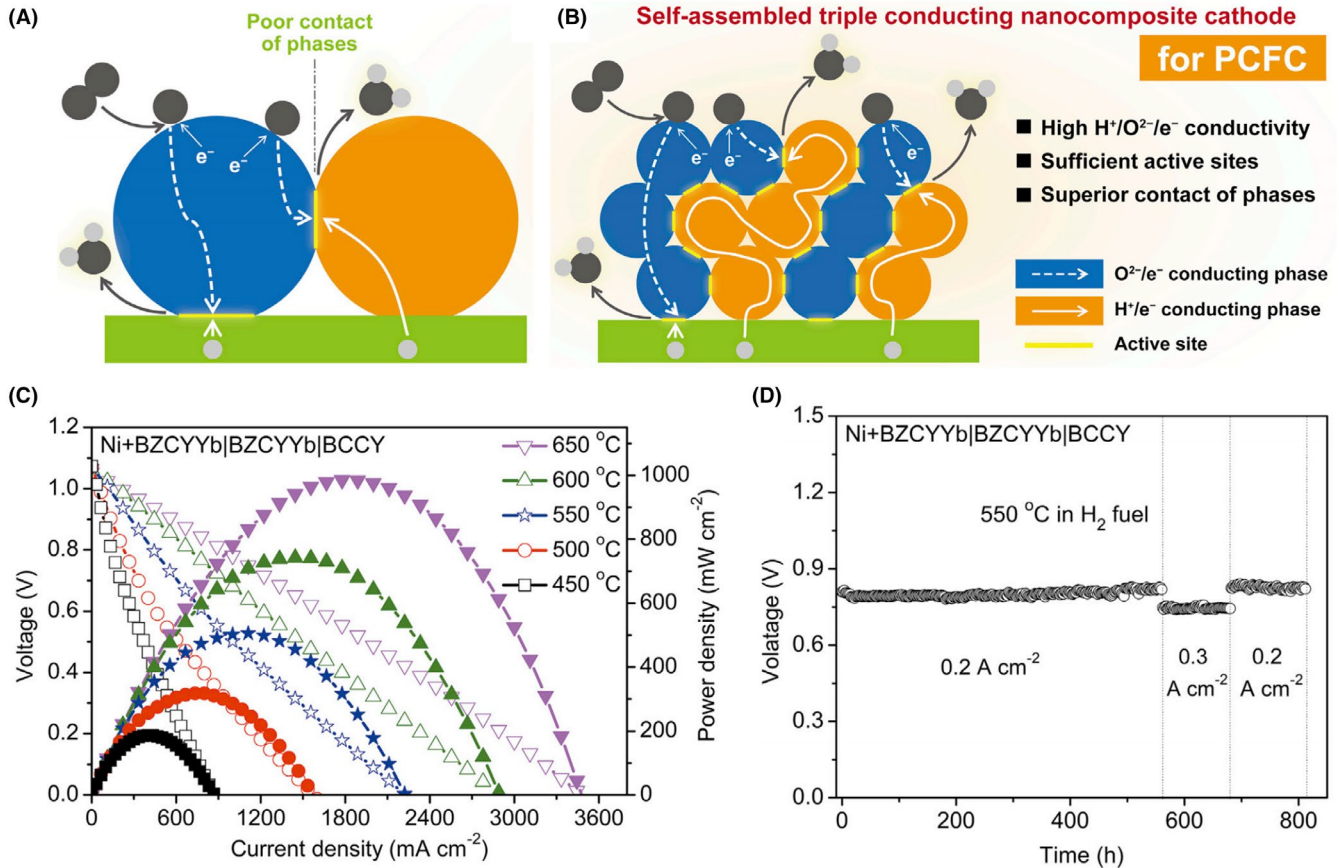


**FIGURE 18** PCFC with conventional triple-conducting cathode (A) and the novel self-assembled triple-conducting nanocomposite cathode (B). Power output (C) and stability test (D) based on a single cell with a configuration of Ni-BZCYYb/BZCYYb/BCCY. (BCCY represents the  $BaCo_{0.7}(Ce_{0.8}Y_{0.2})_{0.3}O_{3-\delta}$ -derived composite cathode). Reprinted with permission from Ref. 194 Copyright 2019 Elsevier

and  $Ba_{0.5}Sr_{0.5}CoO_{3-\delta}$ .<sup>196</sup> For the Ba-containing compounds, the diffusion of elements from cathode to electrolyte induced significant interfacial electronic conduction, extending the electrochemical reaction region. Lin et al evaluated the compatibility of  $Ba_{0.5}Sr_{0.5}Co_{0.8}Fe_{0.2}O_{3-\delta}$  and  $PrBaCo_2O_{5+\delta}$  cathodes with  $BaCeO_3$ -based electrolytes (BCY/BZCY).<sup>197,198</sup> During the heat treatments at 900–1100°C,  $Ba^{2+}$ -enriched BSCF,  $Ba^{2+}$ -deficient BCY,  $Y^{3+}$ -enriched PBC, and  $Co^{3+}$ -enriched BZCY were generated due to the diffusion of cations between electrolytes and cathodes. However, the diffusion of  $Ba^{2+}$  significantly decreased the proton conductivity of the electrolyte due to a significant blocking effect on proton transfer from electrolyte to cathode. The effects of Ba migration at the cathode/electrolyte interface should be further investigated. Besides, some cobaltite-based cathodes have high thermal expansion coefficients that are usually 2–3 times larger than the values of proton-conducting electrolytes.<sup>45</sup> The big difference generally leads to peeling, lamination, and cracking of the fuel cell components, resulting in the degradation of the whole cell system. To address this issue: (1) Partial substitution of Co by other elements (eg, Ni, Cu, and Fe) can mitigate the drawback of Co-containing cathodes, achieving reduced thermal expansion

and maintaining electrochemical activities.<sup>199</sup> (2) The use of cathode-electrolyte combined composite cathodes, as we discussed above, is also an effective method to achieve thermal compatibility.<sup>200</sup> (3) The development of Co-free cathodes, such as  $La_{0.6}Sr_{0.4}Fe_{0.9}Cr_{0.1}O_{3-\delta}$ ,  $PrBaCuFeO_{5+\delta}$ ,  $GdBaCuFeO_{5+\delta}$ , and  $GdBaFeNiO_{5+\delta}$ ,<sup>201–204</sup> are favorable for reducing the cost of materials.

#### 4.3.2 | Anode materials

An anode provides the place for hydrogen oxidation reaction (HOR). Furthermore, hydrocarbons (eg,  $CH_4$ ), which are commonly used as fuels, are converted to hydrogen via reforming in PCFCs. The detailed anode reactions (including the HOR) were illustrated in Figure 19.<sup>205</sup> The anode must meet the following requirements: high activity for fuel oxidation, excellent electronic and protonic conductivity, sufficient porosity and mechanical strength (if the PCFC is anode-supported), and decent chemical/thermal stabilities. The most widely studied PCFC anodes are Ni-based cermet anodes. They are made of Ni with proton-conducting electrolytes to increase the active sites for fuel oxidation and



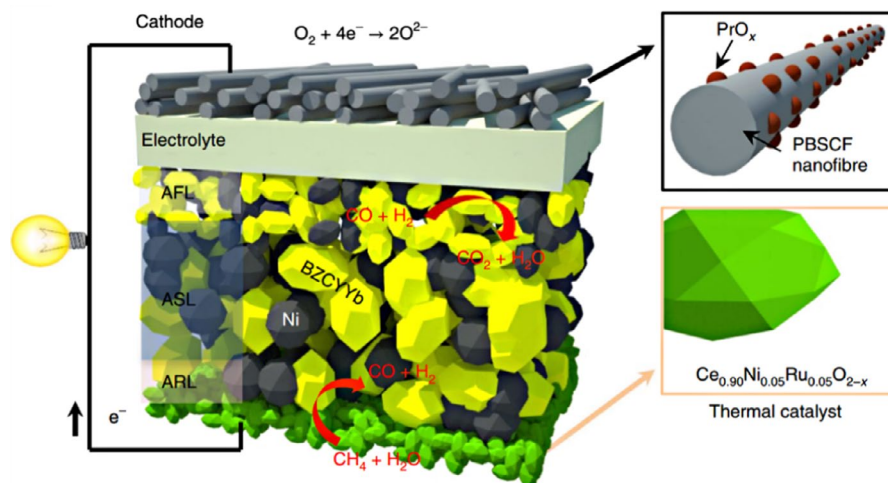


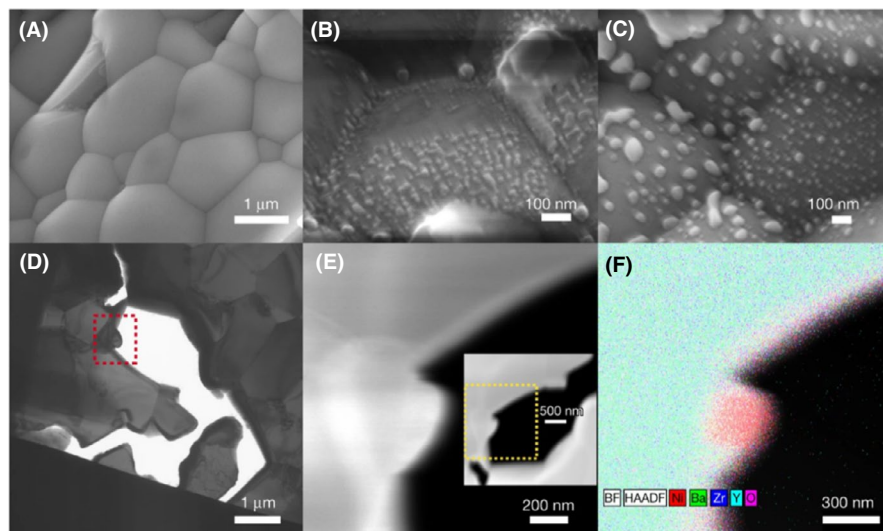
**FIGURE 19** Schematic illustration of a fuel cell device showing the detailed anode reaction processes (AFL: anode functional layer; ASL: anode supporting layer; ARL: anode reforming layer). In the anode,  $\text{CH}_4$  is firstly reformed to  $\text{H}_2$  and  $\text{CO}$  as fuels, followed by the oxidation reactions of  $\text{H}_2$  (HOR) and  $\text{CO}$  at the AFL. Reprinted with permission from Ref. 205 Copyright 2018 Springer Nature

improve the compatibility with electrolytes.<sup>8,206</sup> The state-of-the-art Ni-BZCYyb composite has been identified as an excellent PCFC anode with high catalytic activity and enhanced sulfur and coking tolerance under various hydrocarbon fuels.<sup>156</sup> Compared with oxide-ion-conducting SOFCs, PCFCs are less affected by the porosity of an anode, because water is formed at the cathode and thus less porosity is required for water removal from the anode. A low-porosity (37%) Ni-BZCYyb anode without using the pore former achieved a high-power density of  $1200 \text{ mW cm}^{-2}$  at  $750^\circ\text{C}$  due to sufficient channels of pores formed during the anode reduction.<sup>207</sup> Since the development of Ni-based cermet anodes, especially the mechanism and strategies regarding the tolerance to carbon coking and sulfur poisoning, has been well reviewed in previous literature,<sup>30,208,209</sup> these anodes are not covered here. Therefore, we would like to introduce some new insights on recent development of in situ exsolution techniques for PCFC anodes.

Compared to cathodes, anodes have attracted less attention. Nevertheless, it is important to reduce the anode polarization that causes considerable performance loss at low temperatures. Recent advances in oxide-ion-conducting SOFCs provided feasible strategies for improving the PCFC anode performance. The exsolution of B-site elements from A-deficient perovskite ( $\text{A}_{1-x}\text{BO}_3$ ) can significantly enhance the electrochemical activity of SOFC anodes.<sup>210,211</sup> For example, a composite anode, which consists of  $\text{Pr}_{0.8}\text{Sr}_{1.2}(\text{Co}, \text{Fe})_{0.8}\text{Nb}_{0.2}\text{O}_{4+\delta}$  backbone with homogeneously exsolved Co-Fe nanoparticles, was prepared from perovskite  $\text{Pr}_{0.4}\text{Sr}_{0.6}\text{Co}_{0.2}\text{Fe}_{0.7}\text{Nb}_{0.1}\text{O}_{3-\delta}$  by annealing and hydrogenation, showing almost the same catalytic activity as Ni-based cermet anodes.<sup>210</sup> Similar results were also demonstrated with a perovskite  $\text{Sr}_{0.95}(\text{Ti}_{0.3}\text{Fe}_{0.63}\text{Ni}_{0.07})\text{O}_{3-\delta}$ . Exposure to fuel atmospheres led to exsolution and nucleation of uniformly dispersed Ni-Fe nanoparticles on the original perovskite surface, yielding reduced anode

polarization resistances.<sup>211</sup> Neagu et al further revealed that the in situ exsolved nanoparticles from a perovskite substrate could be well controlled by tuning the stoichiometry of the perovskite, providing an attractive route for tailoring the functions of the resulting products.<sup>212,213</sup> These findings have brought inspirations to the improvement of the anode performance for PCFCs. For instance, Liu et al reported a perovskite  $\text{SrMo}_{0.8}\text{Co}_{0.1}\text{Fe}_{0.1}\text{O}_{3-\delta}$  anode for BZCY-based PCFCs with in situ exsolved Co nanoparticles on the perovskite framework, achieving excellent catalytic activities in hydrogen and ethane.<sup>214</sup> Power densities of  $377 \text{ mW cm}^{-2}$  and  $268 \text{ mW cm}^{-2}$  were achieved at  $750^\circ\text{C}$  using  $\text{H}_2$  and ethane as fuel, respectively. Duan et al observed the exsolution of Ni particles on BZY surface in a Ni-dissolved BZY anode after fuel cell operation. The in situ formed nanocatalyst in the anode during PCFC operation contributed to enhanced catalytic activity and durability in various hydrocarbon fuels (Figure 20).<sup>215</sup> Liu et al developed a new composite anode,  $\text{Ni-Ba}_{0.96}(\text{Ce}_{0.66}\text{Zr}_{0.1}\text{Y}_{0.2}\text{Ni}_{0.04})\text{O}_{3-\delta}$ , with both Ni-doping and A-site deficiency to further facilitate the in situ exsolution of Ni under reducing atmospheres.<sup>216</sup> The anode with exsolved Ni particles achieved higher performances ( $500\text{--}700 \text{ mW cm}^{-2}$ ) at a lower temperature ( $600^\circ\text{C}$ ) compared to the Co-exsolved anode. Furthermore, nanoalloys were also designed as catalysts in perovskite-type oxide anodes (without Ni) to enhance anode performance. Namely, Luo and co-workers prepared a double-layered perovskite  $(\text{Pr}_{0.4}\text{Sr}_{0.6})_3(\text{Fe}_{0.85}\text{Mo}_{0.15})_2\text{O}_7$  anode with in situ exsolved Co-Fe particles via annealing the cubic perovskite  $\text{Pr}_{0.4}\text{Sr}_{0.6}\text{Co}_{0.2}\text{Fe}_{0.7}\text{Mo}_{0.1}\text{O}_{3-\delta}$  under slightly reducing conditions.<sup>217</sup> The highly efficient catalysis of Co-Fe alloy in the anode leads to excellent electrocatalytic activity for ethane-fueled PCFCs, with enhanced cogeneration of ethylene as well. The PCFC device with a BZCY electrolyte achieved peak power densities of  $496.2 \text{ mW cm}^{-2}$  and  $348.84 \text{ mW cm}^{-2}$  at  $750^\circ\text{C}$  in  $\text{H}_2$  and ethane, respectively.<sup>217</sup>

**FIGURE 20** (A) SEM of the as-sintered Ni-containing BZY anode. (B) SEM of the anode after 300 h operation on wet methane under OCV at 600°C. (C) SEM of the anode after 1400 h operation on wet methane under a current density of  $80 \text{ mA cm}^{-2}$  at 500°C. (D) TEM of an extracted sample from area c. The red box is the area to be analyzed in e and f. (E, F) Elemental identification of the anode after fuel cell operation. Reprinted with permission from Ref. 215 Copyright 2018 Springer Nature



## 5 | CONCLUSIONS AND OUTLOOK

The PCFC, which operates at a low temperature with high performance and reliable durability, is a highly promising technology to address the increasing demand for clean energy production. In this article, progress in proton-conducting electrolyte-based PCFCs has been reviewed from material to device aspects, with the following conclusions and perspectives:

Various classes of solid oxide materials, which exhibit intriguing proton-conducting properties, have been explored as electrolytes. The mechanisms of proton conduction were deeply discussed for the commonly used  $A^{2+}B^{4+}O_3$ -type perovskites (eg,  $BaCeO_3$ ,  $BaZrO_3$ -based),  $A^{3+}B^{3+}O_3$ -type perovskites (eg,  $LaScO_3$ -based), perovskite-related proton conductors (eg,  $Ba_3Ca_{1.18}Nb_{1.82}O_{8.73}$ ), and other proton conductors with different crystal structures ( $LaPO_4$ -based,  $RE_{1-x}A_xMO_4$ -structured, etc). Currently, the  $A^{2+}B^{4+}O_3$ -type cerate and zirconate-based perovskites are dominant in practical applications of PCFC devices due to their higher proton conductivity and decent structural stability under optimized conditions. However, the  $A^{3+}B^{3+}O_3$ -type proton conductors (eg, doped  $LaScO_3$ ) have shown their potential to be an alternative to the cerate/zirconate-based materials, especially for enhancing the operational stability of PCFCs. In these  $ABO_3$ -structured proton conductors (both  $A^{2+}B^{4+}O_3$  and  $A^{3+}B^{3+}O_3$ ), protonic defects are generated via absorbed water, where oxide-ion vacancies in these oxides are highly required. Thus, the doping strategy is typically employed to achieve enhanced proton conductivities. Furthermore, the perovskite-related proton conductors provide more opportunities for designing new proton conductors due to their tunable structures, namely, oxygen vacancies can be generated by changing the stoichiometry (eg, increasing the  $B'/B''$  ratio

in the  $A_2(B'B'')O_6$ -type perovskite) to create new proton conductors. Additionally, they are more stable under reducing atmospheres compared with the  $ABO_3$ -type perovskites, showing pure proton conductivity without electronic short-circuit issue. Other proton conductors without a perovskite structure, including phosphates, niobates, and tantalates, have also been developed. In these oxides, charge-compensating proton flow can be formed from water by introducing dopant ions into their crystals. However, limited solubility of dopant ions is a major barrier for increasing their proton conductivities. Overall, the insufficient conductivity of the second and the third types of proton electrolytes limits their applications. Various techniques are expected to improve the conventional and novel proton-conducting oxides for their applications in practical PCFCs, including structural doping, stoichiometry tuning, novel synthesis methods, and processing routes.

There are several critical issues associated with electrolytes in PCFCs, namely, insufficient proton conductivity at low temperatures, nonideal chemical stability under some operating conditions, sinterability, and electron leakage. Codoping strategy has been explored for achieving a balance between high conductivity and sufficient stability. However, sinterability and electron leakage issues deserve more efforts for the fabrication of electrolyte ceramics: (1) Variables that determine the sintered microstructure of compacted powders should be controlled from raw materials to sintering conditions; (2) Besides conventional strategies to inhibit the electron leakage in proton ceramics, the effects of energy band design and alignment mechanism on the elimination of electronic conduction need further studies.

The state-of-the-art BZCY/BZCYYb electrolytes with satisfactory performances (both proton conductivity and chemical stability) have been well developed for PCFC devices. Ni-based cermets are the dominant anodes for PCFCs, even though advanced manufacturing techniques on anodes

are expected to develop efficient alternative anodes. In contrast, triple-conducting cathodes are of diversity, with two major directions of single-phase and composite materials. Doping, hydration, lithiation, and rational design of cation deficiency play important role in tuning the performance of single-phase triple-conducting cathodes. More research efforts are recommended to be made on particle-embedding, in situ exsolution, nano-infiltration, and the facile self-assembly for the fabrication of nanocomposite cathodes for PCFCs. Furthermore, more attentions are expected to the evaluation of proton transport mechanisms in semiconductor electrolytes, where the redox and proton transport occur at oxide interface or surface instead of the bulk.

Finally, challenges regarding scale-up, mass production, long-term stability, and cost-effectiveness need to be solved before the integrated PCFC devices are ready for a commercial assembly line.

## ACKNOWLEDGMENTS

This work was partially supported by National Science Foundation (CMMI-1661699).

## CONFLICT OF INTEREST

There are no conflicts to declare.

## ORCID

Yun Hang Hu  <https://orcid.org/0000-0002-5358-8667>

## REFERENCES

- Brett DJ, Atkinson A, Brandon NP, Skinner SJ. Intermediate temperature solid oxide fuel cells. *Chem Soc Rev.* 2008;37(8):1568-1578.
- Gottesfeld S, Pafford J. A new approach to the problem of carbon monoxide poisoning in fuel cells operating at low temperatures. *J Electrochem Soc.* 1988;135(10):2651-2652.
- Baschuk JJ, Li X. Carbon monoxide poisoning of proton exchange membrane fuel cells. *Int J Energ Res.* 2001;25(8):695-713.
- Sambhy V, Tewari A, Sen A, Macdonald MU. Quantification of carbon dioxide poisoning in air breathing alkaline fuel cells. *ECS Meeting Abstracts.* 2006;MA2005-01:135.
- Au SF, McPhail SJ, Woudstra N, Hemmes K. The influence of operating temperature on the efficiency of a combined heat and power fuel cell plant. *J Power Sources.* 2003;122(1):37-46.
- Su H, Hu YH. Progress in low-temperature solid oxide fuel cells with hydrocarbon fuels. *Chem Eng J.* 2020;402:126235.
- Su H, Hu YH. Recent advances in graphene-based materials for fuel cell applications. *Energy Science and Engineering.* 2021; <https://doi.org/10.1002/ese3.833>
- Goodenough JB, Huang Y-H. Alternative anode materials for solid oxide fuel cells. *J Power Sources.* 2007;173(1):1-10.
- Atkinson A, Barnett S, Gorte RJ, et al. Advanced anodes for high-temperature fuel cells. *Mater Sustain Energy.* 2011;213-223.
- Morita H, Kawase M, Mugikura Y, Asano K. Degradation mechanism of molten carbonate fuel cell based on long-term performance: long-term operation by using bench-scale cell and post-test analysis of the cell. *J Power Sources.* 2010;195(20):6988-6996.
- Fan L, Zhu B, Su P-C, He C. Nanomaterials and technologies for low temperature solid oxide fuel cells: recent advances, challenges and opportunities. *Nano Energy.* 2018;45:148-176.
- Singhal SC. Advances in solid oxide fuel cell technology. *Solid State Ionics.* 2000;135(1-4):305-313.
- Park S, Vohs JM, Gorte RJ. Direct oxidation of hydrocarbons in a solid-oxide fuel cell. *Nature.* 2000;404(6775):265-267.
- Huang P, Horky A, Petric A. Interfacial reaction between nickel oxide and lanthanum gallate during sintering and its effect on conductivity. *J Am Ceram Soc.* 1999;82(9):2402-2406.
- Tietz F. Thermal expansion of SOFC materials. *Ionics.* 1999;5(1-2):129-139.
- Koh J-H, Yoo Y-S, Park J-W, Lim HC. Carbon deposition and cell performance of Ni-YSZ anode support SOFC with methane fuel. *Solid State Ionics.* 2002;149(3-4):157-166.
- Wachsman ED, Lee KT. Lowering the temperature of solid oxide fuel cells. *Science.* 2011;334(6058):935-939.
- Fabbri E, Pergolesi D, Traversa E. Materials challenges toward proton-conducting oxide fuel cells: a critical review. *Chem Soc Rev.* 2010;39(11):4355-4369.
- Nien SH, Hsu CS, Chang CL, Hwang BH. Preparation of BaZr<sub>0.1</sub>Ce<sub>0.7</sub>Y<sub>0.2</sub>O<sub>3-δ</sub> based solid oxide fuel cells with anode functional layers by tape casting. *Fuel Cells.* 2011;11(2):178-183.
- Duan C, Tong J, Shang M, et al. Readily processed protonic ceramic fuel cells with high performance at low temperatures. *Science.* 2015;349(6254):1321-1326.
- Bae K, Jang DY, Choi HJ, et al. Demonstrating the potential of yttrium-doped barium zirconate electrolyte for high-performance fuel cells. *Nat Commun.* 2017;8:14553.
- An H, Lee H-W, Kim B-K, et al. A 5×5 cm<sup>2</sup> protonic ceramic fuel cell with a power density of 1.3 W cm<sup>-2</sup> at 600° C. *Nature Energy.* 2018;3(10):870-875.
- Choi S, Kucharczyk CJ, Liang Y, et al. Exceptional power density and stability at intermediate temperatures in protonic ceramic fuel cells. *Nature Energy.* 2018;3(3):202.
- Liu QL, Khor KA, Chan SH. High-performance low-temperature solid oxide fuel cell with novel BSCF cathode. *J Power Sources.* 2006;161(1):123-128.
- Shao Z, Haile SM. A high-performance cathode for the next generation of solid-oxide fuel cells. *Mater Sustain Energy.* 2011;255-258.
- Gao Z, Moggi LV, Miller EC, Railsback JG, Barnett SA. A perspective on low-temperature solid oxide fuel cells. *Energy Environ Sci.* 2016;9(5):1602-1644.
- Fabbri E, Pergolesi D, D'Epifanio A, et al. Design and fabrication of a chemically-stable proton conductor bilayer electrolyte for intermediate temperature solid oxide fuel cells (IT-SOFCs). *Energy Environ Sci.* 2008;1(3):355-359.
- Norby T, Magrasó A. On the development of proton ceramic fuel cells based on Ca-doped LaNbO<sub>4</sub> as electrolyte. *J Power Sources.* 2015;282:28-33.
- Hossain S, Abdalla AM, Jamain SNB, Zaini JH, Azad AK. A review on proton conducting electrolytes for clean energy and intermediate temperature-solid oxide fuel cells. *Renew Sust Energ Rev.* 2017;79:750-764.
- Dai H, Kou H, Wang H, Bi L. Electrochemical performance of protonic ceramic fuel cells with stable BaZrO<sub>3</sub>-based electrolyte: a mini-review. *Electrochem Commun.* 2018;96:11-15.
- Kim J, Sengodan S, Kim S, Kwon O, Bu Y, Kim G. Proton conducting oxides: a review of materials and applications for



- renewable energy conversion and storage. *Renew Sust Energ Rev.* 2019;109:606-618.
31. Loureiro FJA, Nasani N, Reddy GS, Munirathnam NR, Fagg DP. A review on sintering technology of proton conducting BaCeO<sub>3</sub>-BaZrO<sub>3</sub> perovskite oxide materials for Protonic Ceramic Fuel Cells. *J Power Sources.* 2019;438:226991.
  32. Rashid NLRM, Samat AA, Jais AA, et al. Review on zirconate-cerate-based electrolytes for proton-conducting solid oxide fuel cell. *Ceram Int.* 2019;45(6):6605-6615.
  33. Li J, Wang C, Wang X, Bi L. Sintering aids for proton-conducting oxides—a double-edged sword? A mini review. *Electrochem Commun.* 2020;112:106672.
  34. Iwahara H, Esaka T, Uchida H, Maeda N. Proton conduction in sintered oxides and its application to steam electrolysis for hydrogen production. *Solid State Ionics.* 1981;3:359-363.
  35. Iwahara H. Technological challenges in the application of proton conducting ceramics. *Solid State Ionics.* 1995;77:289-298.
  36. Yajima T, Kazeoka H, Yogo T, Iwahara H. Proton conduction in sintered oxides based on CaZrO<sub>3</sub>. *Solid State Ionics.* 1991;47(3-4):271-275.
  37. Iwahara H. Oxide-ionic and protonic conductors based on perovskite-type oxides and their possible applications. *Solid State Ionics.* 1992;52(1-3):99-104.
  38. Yajima T, Suzuki H, Yogo T, Iwahara H. Protonic conduction in SrZrO<sub>3</sub>-based oxides. *Solid State Ionics.* 1992;51(1-2):101-107.
  39. Iwahara H, Yajima T, Hibino T, Ozaki K, Suzuki H. Protonic conduction in calcium, strontium and barium zirconates. *Solid State Ionics.* 1993;61(1-3):65-69.
  40. Iwahara H. Proton conducting ceramics and their applications. *Solid State Ionics.* 1996;86:9-15.
  41. Katahira K, Kohchi Y, Shimura T, Iwahara H. Protonic conduction in Zr-substituted BaCeO<sub>3</sub>. *Solid State Ionics.* 2000;138(1-2):91-98.
  42. Iwahara H, Uchida H, Ono K, Ogaki K. Proton conduction in sintered oxides based on BaCeO<sub>3</sub>. *J Electrochem Soc.* 1988;135(2):529-533.
  43. Shin S, Huang HH, Ishigame M, Iwahara H. Protonic conduction in the single crystals of SrZrO<sub>3</sub> and SrCeO<sub>3</sub> doped with Y<sub>2</sub>O<sub>3</sub>. *Solid State Ionics.* 1990;40:910-913.
  44. Slade RCT, Singh N. The perovskite-type proton-conducting solid electrolyte BaCe<sub>0.90</sub>Y<sub>0.10</sub>O<sub>3-α</sub> in high temperature electrochemical cells. *Solid State Ionics.* 1993;61(1-3):111-114.
  45. Medvedev D, Murashkina A, Pikalova E, Demin A, Podias A, Tsiakaras P. BaCeO<sub>3</sub>: Materials development, properties and application. *Prog Mater Sci.* 2014;60:72-129.
  46. Wienströer S, Wiemhöfer HD. Investigation of the influence of zirconium substitution on the properties of neodymium-doped barium cerates. *Solid State Ionics.* 1997;101:1113-1117.
  47. Haile SM, Stanoff G, Ryu KH. Non-stoichiometry, grain boundary transport and chemical stability of proton conducting perovskites. *J Mater Sci.* 2001;36(5):1149-1160.
  48. Zuo C, Zha S, Liu M, Hatano M, Uchiyama M. Ba (Zr<sub>0.1</sub>Ce<sub>0.7</sub>Y<sub>0.2</sub>)O<sub>3-δ</sub> as an electrolyte for low-temperature solid-oxide fuel cells. *Adv Mater.* 2006;18(24):3318-3320.
  49. Tao S, Irvine JTS. Conductivity studies of dense yttrium-doped BaZrO<sub>3</sub> sintered at 1325°C. *J Solid State Chem.* 2007;180(12):3493-3503.
  50. Ahmed I, Karlsson M, Eriksson SG, et al. Crystal structure and proton conductivity of BaZr<sub>0.9</sub>Sc<sub>0.1</sub>O<sub>3-δ</sub>. *J Am Ceram Soc.* 2008;91(9):3039-3044.
  51. Azad AK, Savaniu C, Tao S, et al. Structural origins of the differing grain conductivity values in BaZr<sub>0.9</sub>Y<sub>0.1</sub>O<sub>2.95</sub> and indication of novel approach to counter defect association. *J Mater Chem.* 2008;18(29):3414-3418.
  52. Bilić A, Gale JD. Ground state structure of BaZrO<sub>3</sub>: a comparative first-principles study. *Phys Rev B.* 2009;79(17):174107.
  53. Fabbri E, Pergolesi D, Licocchia S, Traversa E. Does the increase in Y-dopant concentration improve the proton conductivity of BaZr<sub>1-x</sub>Y<sub>x</sub>O<sub>3-δ</sub> fuel cell electrolytes? *Solid State Ionics.* 2010;181(21-22):1043-1051.
  54. Khani Z, Taillades-Jacquín M, Taillades G, Jones DJ, Marrony M, Roziere J. Preparation of nanoparticle core-shell electrolyte materials for proton ceramic fuel cells. *Chem Mater.* 2010;22(3):1119-1125.
  55. Ryu KH, Haile SM. Chemical stability and proton conductivity of doped BaCeO<sub>3</sub>-BaZrO<sub>3</sub> solid solutions. *Solid State Ionics.* 1999;125(1-4):355-367.
  56. Zhang Y, Zha S, Liu M. Dual-scale porous electrodes for solid oxide fuel cells from polymer foams. *Adv Mater.* 2005;17:487-491.
  57. Larring Y, Norby T. Protons in LaErO<sub>3</sub>. *Solid State Ionics.* 1994;70:305-310.
  58. Ruiz-Trejo E, Kilner JA. Oxygen diffusion and proton conduction in La<sub>1-x</sub>Sr<sub>x</sub>YO<sub>3-δ</sub>. *Solid State Ionics.* 1997;97(1-4):529-534.
  59. Lybye D, Bonanos N. Proton and oxide ion conductivity of doped LaScO<sub>3</sub>. *Solid State Ionics.* 1999;125(1-4):339-344.
  60. Nomura K, Takeuchi T, Tanase S, Kageyama H, Tanimoto K, Miyazaki Y. Proton conduction in (La<sub>0.9</sub>Sr<sub>0.1</sub>) MIII O<sub>3-δ</sub> (MIII= Sc, In, and Lu) perovskites. *Solid State Ionics.* 2002;154:647-652.
  61. Münch W, Kreuer KD, St A, Seifert G, Maier J. The relation between crystal structure and the formation and mobility of protonic charge carriers in perovskite-type oxides: a case study of Y-doped BaCeO<sub>3</sub> and SrCeO<sub>3</sub>. *Phase Transit.* 1999;68(3):567-586.
  62. Nomura K, Takeuchi T, Kamo S-I, Kageyama H, Miyazaki Y. Proton conduction in doped LaScO<sub>3</sub> perovskites. *Solid State Ionics.* 2004;175(1-4):553-555.
  63. Hibino T, Mizutani K, Yajima T, Iwahara H. Evaluation of proton conductivity in SrCeO<sub>3</sub>, BaCeO<sub>3</sub>, CaZrO<sub>3</sub> and SrZrO<sub>3</sub> by temperature programmed desorption method. *Solid State Ionics.* 1992;57(3-4):303-306.
  64. Liang KC, Du Y, Nowick AS. Fast high-temperature proton transport in nonstoichiometric mixed perovskites. *Solid State Ionics.* 1994;69(2):117-120.
  65. Singh K, Kan WH, Patton B, Huq A, Thangadurai V. Insights into B-site ordering in double perovskite-type Ba<sub>3</sub>Ca<sub>1+x</sub>Nb<sub>2-x</sub>O<sub>9-8</sub> (0 ≤ x ≤ 0.45): combined synchrotron and neutron diffraction and electrical transport analyses. *Inorg Chem.* 2018;57(5):2609-2619.
  66. Animitsa I, Neiman A, Sharafutdinov A, Nochrin S. Strontium tantalates with perovskite-related structure. *Solid State Ionics.* 2000;136:265-271.
  67. Animitsa I, Nieman A, Titova S, et al. Phase relations during water incorporation in the oxygen and proton conductor Sr<sub>6</sub>Ta<sub>2</sub>O<sub>11</sub>. *Solid State Ionics.* 2003;156(1-2):95-102.
  68. Fisher CAJ, Islam MS. Defect, protons and conductivity in brownmillerite-structured Ba<sub>2</sub>In<sub>2</sub>O<sub>5</sub>. *Solid State Ionics.* 1999;118(3-4):355-363.
  69. Mohn CE, Allan NL, Freeman CL, Ravindran P, Stølen S. Collective ionic motion in oxide fast-ion-conductors. *Phys Chem Chem Phys.* 2004;6(12):3052-3055.



70. Mohn CE, Allan NL, Freeman CL, Ravindran P, Stølen S. Order in the disordered state: local structural entities in the fast ion conductor  $\text{Ba}_2\text{In}_2\text{O}_5$ . *J Solid State Chem.* 2005;178(1):346-355.
71. Noirault S, Celerier S, Joubert O, Caldes MT, Piffard Y. Water incorporation into the  $(\text{Ba}_{1-x}\text{La}_x)_2\text{In}_2\text{O}_{5+x}\square_{1-x}$  ( $0 \leq x < 0.6$ ) system. *Solid State Ionics.* 2007;178(23-24):1353-1359.
72. Shin JF, Hussey L, Orera A, Slater PR. Enhancement of the conductivity of  $\text{Ba}_2\text{In}_2\text{O}_5$  through phosphate doping. *Chem Commun.* 2010;46(25):4613-4615.
73. Goodenough JB, Ruiz-Diaz JE, Zhen YS. Oxide-ion conduction in  $\text{Ba}_2\text{In}_2\text{O}_5$  and  $\text{Ba}_3\text{In}_2\text{MO}_8$  (M= Ce, Hf, or Zr). *Solid State Ionics.* 1990;44(1-2):21-31.
74. Speakman SA, Richardson JW, Mitchell BJ, Misture ST. In-situ diffraction study of  $\text{Ba}_2\text{In}_2\text{O}_5$ . *Solid State Ionics.* 2002;149(3-4):247-259.
75. Kakinuma K, Tomita A, Yamamura H, Atake T. Water vapor absorption and proton conductivity of  $(\text{Ba}_{1-x}\text{La}_x)_2\text{In}_2\text{O}_{5+x}$ . *J Mater Sci.* 2006;41(19):6435-6440.
76. Quarez E, Noirault S, Caldes MT, Joubert O. Water incorporation and proton conductivity in titanium substituted barium indate. *J Power Sources.* 2010;195(4):1136-1141.
77. Paschos O, Kunze J, Stimming U, Maglia F. A review on phosphate based, solid state, protonic conductors for intermediate temperature fuel cells. *J Phys: Condens Matter.* 2011;23:234110.
78. Greenblatt M, Tsai PP, Kodama T, Tanase S. Humidity sensor with sintered  $\beta\text{-Ca}(\text{PO}_3)_2$  for high temperature use. *Solid State Ionics.* 1990;40:444-447.
79. Mellander BE, Zhu B. High temperature protonic conduction in phosphate-based salts. *Solid State Ionics.* 1993;61(1-3):105-110.
80. Norby T, Christiansen N. Proton conduction in Ca- and Sr-substituted  $\text{LaPO}_4$ . *Solid State Ionics.* 1995;77:240-243.
81. Amezawa K, Tomii Y, Yamamoto N. High-temperature protonic conduction in  $\text{La}_7\text{P}_3\text{O}_{18}$ . *Solid State Ionics.* 2004;175(1-4):569-573.
82. Amezawa K, Kitajima Y, Tomii Y, Yamamoto N, Widerøe M, Norby T. Protonic conduction in acceptor-doped  $\text{LaP}_3\text{O}_9$ . *Solid State Ionics.* 2005;176(39-40):2867-2870.
83. Li S, Schönberger F, Slater P.  $\text{La}_{1-x}\text{Ba}_{1+x}\text{GaO}_{4-x/2}$ : a novel high temperature proton conductor. *Chem Commun.* 2003;21:2694-2695.
84. Kendrick E, Kendrick J, Knight KS, Islam MS, Slater PR. Cooperative mechanisms of fast-ion conduction in gallium-based oxides with tetrahedral moieties. *Nature Mater.* 2007;6(11):871-875.
85. Haugsrud R, Norby T. Proton conduction in rare-earth orthoniobates and ortho-tantalates. *Nature Mater.* 2006;5(3):193-196.
86. Kreuer K-D. Proton-conducting oxides. *Ann Rev Mater Res.* 2003;33(1):333-359.
87. Malavasi L, Fisher CAJ, Islam MS. Oxide-ion and proton conducting electrolyte materials for clean energy applications: structural and mechanistic features. *Chem Soc Rev.* 2010;39(11):4370-4387.
88. Yamaguchi S, Yamada N. Thermal lattice expansion behavior of Yb-doped  $\text{BaCeO}_3$ . *Solid State Ionics.* 2003;162:23-29.
89. Sharova NV, Gorelov VP. Characteristics of Proton-conducting electrolytes  $\text{BaCe}_{1-x}\text{Nd}_x\text{O}_{3-\delta}$  ( $0 \leq x \leq 0.16$ ) in moist air. *Russ J Electrochem.* 2005;41(9):1001-1007.
90. Maffei N, Pelletier L, Charland JP, McFarlan A. An ammonia fuel cell using a mixed ionic and electronic conducting electrolyte. *J Power Sources.* 2006;162(1):165-167.
91. Wang MY, Qiu LG, Ma GL. Ionic conduction in  $\text{Ba}_{0.95}\text{Ce}_{0.8}\text{Ho}_{0.2}\text{O}_{3-\alpha}$ . *Chin J Chem.* 2007;25(9):1273-1277.
92. Gorbova E, Maragou V, Medvedev D, Demin A, Tsiakaras P. Investigation of the protonic conduction in Sm doped  $\text{BaCeO}_3$ . *J Power Sources.* 2008;181(2):207-213.
93. Wang M-Y, Qiu L-G. Mixed Conduction in  $\text{BaCe}_{0.8}\text{Pr}_{0.2}\text{O}_{3-\alpha}$  Ceramic. *Chin. J Chem Phys.* 2008;21(3):286.
94. Chen C, Ma G. Proton conduction in  $\text{BaCe}_{1-x}\text{Gd}_x\text{O}_{3-\alpha}$  at intermediate temperature and its application to synthesis of ammonia at atmospheric pressure. *J Alloy Compd.* 2009;485(1-2):69-72.
95. Matskevich NI, Wolf T, Matskevich MY, Chupakhina TI. Preparation, stability and thermodynamic properties of Nd- and Lu-Doped  $\text{BaCeO}_3$  proton-conducting ceramics. *Eur J Inorg Chem.* 2009;11:1477-1482.
96. Matskevich NI, Wolf TA. The enthalpies of formation of  $\text{BaCe}_{1-x}\text{RE}_x\text{O}_{3-\delta}$  (RE= Eu, Tb, Gd). *J Chem Thermodyn.* 2010;42(2):225-228.
97. Qiu L-G, Wang M-Y. Ionic conduction and fuel cell performance of  $\text{Ba}_{0.98}\text{Ce}_{0.8}\text{Tm}_{0.2}\text{O}_{3-\alpha}$  ceramic. *Chin J Chem Phys.* 2010;23(6):707.
98. Wang WB, Liu JW, Li YD, Wang HT, Zhang F, Ma GL. Microstructures and proton conduction behaviors of Dy-doped  $\text{BaCeO}_3$  ceramics at intermediate temperature. *Solid State Ionics.* 2010;181(15-16):667-671.
99. Yin J, Wang X, Xu J, Wang H, Zhang F, Ma G. Ionic conduction in  $\text{BaCe}_{0.85-x}\text{Zr}_x\text{Er}_{0.15}\text{O}_{3-\alpha}$  and its application to ammonia synthesis at atmospheric pressure. *Solid State Ionics.* 2011;185(1):6-10.
100. Kilner JA. Fast oxygen transport in acceptor doped oxides. *Solid State Ionics.* 2000;129(1-4):13-23.
101. Amsif M, Marrero-Lopez D, Ruiz-Morales JC, Savvin SN, Gabás M, Nunez P. Influence of rare-earth doping on the microstructure and conductivity of  $\text{BaCe}_{0.9}\text{Ln}_{0.1}\text{O}_{3-\delta}$  proton conductors. *J Power Sources.* 2011;196(7):3461-3469.
102. Zhao F, Chen F. Performance of solid oxide fuel cells based on proton-conducting  $\text{BaCe}_{0.7}\text{In}_{0.3-x}\text{Y}_x\text{O}_{3-\delta}$  electrolyte. *Int J Hydrogen Energ.* 2010;35(20):11194-11199.
103. Bi L, Zhang S, Zhang L, Tao Z, Wang H, Liu W. Indium as an ideal functional dopant for a proton-conducting solid oxide fuel cell. *Int J Hydrogen Energ.* 2009;34(5):2421-2425.
104. Zhang C, Zhao H. Influence of In content on the electrical conduction behavior of Sm- and In-co-doped proton conductor  $\text{BaCe}_{0.80-x}\text{Sm}_{0.20}\text{In}_x\text{O}_{3-\delta}$ . *Solid State Ionics.* 2012;206:17-21.
105. Su X-T, Yan Q-Z, Ma X-H, Zhang W-F, Ge C-C. Effect of co-dopant addition on the properties of yttrium and neodymium doped barium cerate electrolyte. *Solid State Ionics.* 2006;177(11-12):1041-1045.
106. Lee Y-C, Hung IM, Chang S-L, Ciou C-J, Wu J-S. The effects of doped Nd on conductivity and phase stability of  $\text{BaCe}_{0.8}\text{Y}_{0.2}\text{O}_{3-\delta}$ -based electrolyte for solid oxide fuel cell. *J Eur Ceram Soc.* 2011;31(16):3137-3143.
107. Fu X-Z, Luo J-L, Sanger AR, Danilovic N, Chuang KT. An integral proton conducting SOFC for simultaneous production of ethylene and power from ethane. *Chem Commun.* 2010;46(12):2052-2054.
108. Zhang C, Zhao H. Electrical conduction behavior of Sr substituted proton conductor  $\text{Ba}_{1-x}\text{Sr}_x\text{Ce}_{0.9}\text{Nd}_{0.1}\text{O}_{3-\delta}$ . *Solid State Ionics.* 2010;181(33-34):1478-1485.
109. Gopalan S, Virkar AV. Thermodynamic stabilities of  $\text{SrCeO}_3$  and  $\text{BaCeO}_3$  using a molten salt method and galvanic cells. *J Electrochem Soc.* 1993;140(4):1060-1065.

110. Bhide SV, Virkar AV. Stability of BaCeO<sub>3</sub>-based proton conductors in water-containing atmospheres. *J Electrochem Soc.* 1999;146(6):2038-2044.
111. Radojković A, Žunić M, Savić SM, Branković G, Branković Z. Chemical stability and electrical properties of Nb doped BaCe<sub>0.9</sub>Y<sub>0.1</sub>O<sub>3-δ</sub> as a high temperature proton conducting electrolyte for IT-SOFC. *Ceram Int.* 2013;39(1):307-313.
112. Xie K, Yan R, Chen X, et al. A new stable BaCeO<sub>3</sub>-based proton conductor for intermediate-temperature solid oxide fuel cells. *J Alloy Compd.* 2009;472(1-2):551-555.
113. Xie K, Yan R, Xu X, Liu X, Meng G. A stable and thin BaCe<sub>0.7</sub>Nb<sub>0.1</sub>Gd<sub>0.2</sub>O<sub>3-δ</sub> membrane prepared by simple all-solid-state process for SOFC. *J Power Sources.* 2009;187(2):403-406.
114. Xie K, Yan R, Chen X, et al. A stable and easily sintering BaCeO<sub>3</sub>-based proton-conductive electrolyte. *J Alloy Compd.* 2009;473(1-2):323-329.
115. Yan R, Wang Q, Chen G, Huang W, Xie K. A stable BaCeO<sub>3</sub>-based proton conductor for solid oxide fuel cells. *Ionic.* 2009;15(6):749.
116. Liu X-M, Gu Y-J, Liu Z-G, Ouyang J-H, Yan F-YY, Xiang J. Electrical conductivity and chemical stability of BaCe<sub>0.8-x</sub>A<sub>x</sub>Gd<sub>0.2</sub>O<sub>3-δ</sub> (A = In, Zr, Ta; x = 0, 0.1) ceramics. *B Mater Sci.* 2013;36(3):395-401.
117. Iguchi F, Tsurui T, Sata N, Nagao Y, Yugami H. The relationship between chemical composition distributions and specific grain boundary conductivity in Y-doped BaZrO<sub>3</sub> proton conductors. *Solid State Ionics.* 2009;180(6-8):563-568.
118. Li Y, Guo R, Wang C, et al. Stable and easily sintered BaCe<sub>0.5</sub>Zr<sub>0.3</sub>Y<sub>0.2</sub>O<sub>3-δ</sub> electrolytes using ZnO and Na<sub>2</sub>CO<sub>3</sub> additives for protonic oxide fuel cells. *Electrochim Acta.* 2013;95:95-101.
119. Azad A-M, Subramaniam S, Dung TW. On the development of high density barium metazirconate (BaZrO<sub>3</sub>) ceramics. *J Alloy Compd.* 2002;334(1-2):118-130.
120. Duval SBC, Holtappels P, Stimming U, Graule T. Effect of minor element addition on the electrical properties of BaZr<sub>0.9</sub>Y<sub>0.1</sub>O<sub>3-δ</sub>. *Solid State Ionics.* 2008;179(21-26):1112-1115.
121. Costa R, Grünbaum N, Berger MH, Dessemond L, Thorel A. On the use of NiO as sintering additive for BaCe<sub>0.9</sub>Y<sub>0.1</sub>O<sub>3-δ</sub>. *Solid State Ionics.* 2009;180(11-13):891-895.
122. Zhang M, Xu J, Ma G. Proton conduction in Ba<sub>x</sub>Ce<sub>0.8</sub>Y<sub>0.2</sub>O<sub>3-α</sub>+0.04ZnO at intermediate temperatures and its application in ammonia synthesis at atmospheric pressure. *J Mater Sci.* 2011;46(13):4690-4694.
123. Fabbri E, Bi L, Rupp JLM, Pergolesi D, Traversa E. Electrode tailoring improves the intermediate temperature performance of solid oxide fuel cells based on a Y and Pr co-doped barium zirconate proton conducting electrolyte. *RSC Adv.* 2011;1(7):1183-1186.
124. Jiang T, Liu Y, Wang Z, Sun W, Qiao J, Sun K. An improved direct current sintering technique for proton conductor-BaZr<sub>0.1</sub>Ce<sub>0.7</sub>Y<sub>0.1</sub>Yb<sub>0.1</sub>O<sub>3</sub>: The effect of direct current on sintering process. *J Power Sources.* 2014;248:70-76.
125. Petit CTG, Tao S. Structural, thermal and electrical properties of Bi and Y co-doped barium zirconium cerates. *Ionic.* 2014;20(3):363-371.
126. Qian J, Sun W, Zhang Q, Jiang G, Liu W. Fabrication and performance of BaCe<sub>0.8</sub>Y<sub>0.2</sub>O<sub>3-δ</sub>-BaZr<sub>0.8</sub>Y<sub>0.2</sub>O<sub>3-δ</sub> bilayer electrolyte for anode-supported solid oxide fuel cells. *J Power Sources.* 2014;249:131-136.
127. Radojković A, Savić SM, Pršić S, Branković Z, Branković G. Improved electrical properties of Nb doped BaCe<sub>0.9</sub>Y<sub>0.1</sub>O<sub>2.95</sub> electrolyte for intermediate temperature SOFCs obtained by autocombustion method. *J Alloy Compd.* 2014;583:278-284.
128. Shi Z, Sun W, Wang Z, Qian J, Liu W. Samarium and yttrium codoped BaCeO<sub>3</sub> proton conductor with improved sinterability and higher electrical conductivity. *ACS Appl Mater Inter.* 2014;6(7):5175-5182.
129. Liu Y, Ran R, Tade MO, Shao Z. Structure, sinterability, chemical stability and conductivity of proton-conducting BaZr<sub>0.6</sub>M<sub>0.2</sub>Y<sub>0.2</sub>O<sub>3-δ</sub> electrolyte membranes: the effect of the M dopant. *J Membrane Sci.* 2014;467:100-108.
130. Gu Y-J, Liu Z-G, Ouyang J-H, Yan F-Y, Zhou Y. Structure and electrical conductivity of BaCe<sub>0.85</sub>Ln<sub>0.15</sub>O<sub>3-δ</sub> (Ln = Gd, Y, Yb) ceramics. *Electrochim Acta.* 2013;105:547-553.
131. Zhao F, Liu Q, Wang S, Brinkman K, Chen F. Synthesis and characterization of BaIn<sub>0.3-x</sub>Y<sub>x</sub>Ce<sub>0.7</sub>O<sub>3-δ</sub> (x = 0, 0.1, 0.2, 0.3) proton conductors. *Int J Hydrogen Energy.* 2010;35(9):4258-4263.
132. Wan Y, He B, Wang R, Ling Y, Zhao L. Effect of Co doping on sinterability and protonic conductivity of BaZr<sub>0.1</sub>Ce<sub>0.7</sub>Y<sub>0.1</sub>Yb<sub>0.1</sub>O<sub>3-δ</sub> for protonic ceramic fuel cells. *J Power Sources.* 2017;347:14-20.
133. Zhu Z, Wang S. Investigation on samarium and yttrium co-doping barium zirconate proton conductors for protonic ceramic fuel cells. *Ceram Int.* 2019;45(15):19289-19296.
134. Uchida H, Maeda N, Iwahara H. Relation between proton and hole conduction in SrCeO<sub>3</sub>-based solid electrolytes under water-containing atmospheres at high temperatures. *Solid State Ionics.* 1983;11(2):117-124.
135. Schober T, Schilling W, Wenzl H. Defect model of proton insertion into oxides. *Solid State Ionics.* 1996;86:653-658.
136. Norby T, Larring Y. Concentration and transport of protons in oxides. *Curr Opin Solid St M.* 1997;2(5):593-599.
137. Poulsen FW. Method for calculating ionic and electronic defect concentrations in proton containing perovskites. *J Solid State Chem.* 1999;143(1):115-121.
138. Stokes SJ, Islam MS. Defect chemistry and proton-dopant association in BaZrO<sub>3</sub> and BaPrO<sub>3</sub>. *J Mater Chem.* 2010;20(30):6258-6264.
139. Hermet J, Bottin F, Dezanneau G, Geneste G. Thermodynamics of hydration and oxidation in the proton conductor Gd-doped barium cerate from density functional theory calculations. *Phys Rev B.* 2012;85(20):205137.
140. Kim D-Y, Miyoshi S, Tsuchiya T, Yamaguchi S. Electronic defect formation in Fe-doped BaZrO<sub>3</sub> studied by X-ray absorption spectroscopy. *Chem Mater.* 2014;26(2):927-934.
141. Bonanos N. Transport properties and conduction mechanism in high-temperature protonic conductors. *Solid State Ionics.* 1992;53:967-974.
142. Nakamura T, Mizunuma S, Kimura Y, et al. Energy efficiency of ionic transport through proton conducting ceramic electrolytes for energy conversion applications. *J Mater Chem A.* 2018;6(32):15771-15780.
143. Sun W, Shi Z, Qian J, Wang Z, Liu W. In-situ formed Ce<sub>0.8</sub>Sm<sub>0.2</sub>O<sub>2-δ</sub>@Ba(Ce, Zr)<sub>1-x</sub>(Sm, Y)<sub>x</sub>O<sub>3-δ</sub> core/shell electron-blocking layer towards Ce<sub>0.8</sub>Sm<sub>0.2</sub>O<sub>2-δ</sub>-based solid oxide fuel cells with high open circuit voltages. *Nano Energy.* 2014;8:305-311.
144. Sun W, Shi Z, Wang Z, Liu W. Bilayered BaZr<sub>0.1</sub>Ce<sub>0.7</sub>Y<sub>0.2</sub>O<sub>3-δ</sub>/Ce<sub>0.8</sub>Sm<sub>0.2</sub>O<sub>2-δ</sub> electrolyte membranes for solid oxide fuel cells with high open circuit voltages. *J Membrane Sci.* 2015;476:394-398.
145. Dippon M, Babiniec SM, Ding H, Ricote S, Sullivan NP. Exploring electronic conduction through BaCe<sub>x</sub>Zr<sub>0.9-x</sub>Y<sub>0.1</sub>O<sub>3-δ</sub> proton-conducting ceramics. *Solid State Ionics.* 2016;286:117-121.

146. Iwahara H, Uchida H, Tanaka S. High temperature type proton conductor based on  $\text{SrCeO}_3$  and its application to solid electrolyte fuel cells. *Solid State Ionics*. 1983;9:1021-1025.
147. Bonano N, Ellis B, Mahmood MN. Construction and operation of fuel cells based on the solid electrolyte  $\text{BaCeO}_3$ : Gd. *Solid State Ionics*. 1991;44(3-4):305-311.
148. Bi L, Da'as EH, Shafi SP. Proton-conducting solid oxide fuel cell (SOFC) with Y-doped  $\text{BaZrO}_3$  electrolyte. *Electrochem Commun*. 2017;80:20-23.
149. Shi R, Liu J, Wang H, Wu F, Miao H. Intermediate temperature fuel cell durability of Eu-doped  $\text{SrCeO}_3$ - $\text{SrZrO}_3$  solid solution/ $\text{NaCl-KCl}$  composite electrolyte. *Ceram Int*. 2017;43(18):16931-16935.
150. Zajac W, Rusinek D, Zheng K, Molenda J. Applicability of Gd-doped  $\text{BaZrO}_3$ ,  $\text{SrZrO}_3$ ,  $\text{BaCeO}_3$  and  $\text{SrCeO}_3$  proton conducting perovskites as electrolytes for solid oxide fuel cells. *Open Chem*. 2013;11(4):471-484.
151. Zunic M, Chevallier L, Deganello F, et al. Electrophoretic deposition of dense  $\text{BaCe}_{0.9}\text{Y}_{0.1}\text{O}_{3-x}$  electrolyte thick-films on Ni-based anodes for intermediate temperature solid oxide fuel cells. *J Power Sources*. 2009;190(2):417-422.
152. Bi L, Fabbri E, Sun Z, Traversa E. A novel ionic diffusion strategy to fabricate high-performance anode-supported solid oxide fuel cells (SOFCs) with proton-conducting Y-doped  $\text{BaZrO}_3$  films. *Energ Environ Sci*. 2011;4(2):409-412.
153. Lee S, Park I, Lee H, Shin D. Continuously gradient anode functional layer for BCZY based proton-conducting fuel cells. *Int J Hydrogen Energ*. 2014;39(26):14342-14348.
154. Fan L, Su P-C. Layer-structured  $\text{LiNi}_{0.8}\text{Co}_{0.2}\text{O}_2$ : A new triple ( $\text{H}^+/\text{O}^{2-}/\text{e}^-$ ) conducting cathode for low temperature proton conducting solid oxide fuel cells. *J Power Sources*. 2016;306:369-377.
155. Yuan R-H, He W, Zhang C, Ni M, Leung MKH. Cobalt free  $\text{SrFe}_{0.95}\text{Nb}_{0.05}\text{O}_{3-\delta}$  cathode material for proton-conducting solid oxide fuel cells with  $\text{BaZr}_{0.1}\text{Ce}_{0.7}\text{Y}_{0.2}\text{O}_{3-\delta}$  electrolyte. *Mater Lett*. 2017;200:75-78.
156. Yang L, Wang S, Blinn K, et al. Enhanced sulfur and coking tolerance of a mixed ion conductor for SOFCs:  $\text{BaZr}_{0.1}\text{Ce}_{0.7}\text{Y}_{0.2-x}\text{Yb}_x\text{O}_{3-\delta}$ . *Science*. 2009;326(5949):126-129.
157. Kim J, Sengodan S, Kwon G, et al. Triple-conducting layered perovskites as cathode materials for proton-conducting solid oxide fuel cells. *Chemosuschem*. 2014;7(10):2811-2815.
158. Chen C, Dong Y, Li L, et al. Electrochemical properties of micro-tubular intermediate temperature solid oxide fuel cell with novel asymmetric structure based on  $\text{BaZr}_{0.1}\text{Ce}_{0.7}\text{Y}_{0.1}\text{Yb}_{0.1}\text{O}_{3-\delta}$  proton conducting electrolyte. *Int J Hydrogen Energ*. 2019;44(31):16887-16897.
159. Chen C, Dong Y, Li L, et al. High performance of anode supported  $\text{BaZr}_{0.1}\text{Ce}_{0.7}\text{Y}_{0.1}\text{Yb}_{0.1}\text{O}_{3-\delta}$  proton-conducting electrolyte micro-tubular cells with asymmetric structure for IT-SOFCs. *J Electroanal Chem*. 2019;844:49-57.
160. Zhou Y, Guan X, Zhou H, et al. Strongly correlated perovskite fuel cells. *Nature*. 2016;534(7606):231-234.
161. Chen G, Liu H, He Y, et al. Electrochemical mechanisms of an advanced low-temperature fuel cell with a  $\text{SrTiO}_3$  electrolyte. *J Mater Chem A*. 2019;7(16):9638-9645.
162. Dong W, Tong Y, Zhu B, et al. Semiconductor  $\text{TiO}_2$  thin film as an electrolyte for fuel cells. *J Mater Chem A*. 2019;7(28):16728-16734.
163. Wang B, Zhu B, Yun S, et al. Fast ionic conduction in semiconductor  $\text{CeO}_{2-\delta}$  electrolyte fuel cells. *NPG Asia Mater*. 2019;11(1):1-12.
164. Xia C, Mi Y, Wang B, Lin B, Chen G, Zhu B. Shaping triple-conducting semiconductor  $\text{BaCo}_{0.4}\text{Fe}_{0.4}\text{Zr}_{0.1}\text{Y}_{0.1}\text{O}_{3-\delta}$  into an electrolyte for low-temperature solid oxide fuel cells. *Nat Commun*. 2019;10(1):1707.
165. Xing Y, Wu Y, Li L, et al. Proton shuttles in  $\text{CeO}_2/\text{CeO}_{2-\delta}$  core-shell structure. *ACS Energy Lett*. 2019;4(11):2601-2607.
166. Shah MAKY, Zhu B, Rauf S, et al. Electrochemical properties of a co-doped  $\text{SrSnO}_{3-\delta}$ -based semiconductor as an electrolyte for solid oxide fuel cells. *ACS Appl Energy Mater*. 2020;3(7):6323-6333.
167. Wu Y, Zhu B, Huang M, et al. Proton transport enabled by a field-induced metallic state in a semiconductor heterostructure. *Science*. 2020;369(6500):184-188.
168. Lan R, Tao S. Novel proton conductors in the layered oxide material  $\text{Li}_x\text{Al}_{0.5}\text{Co}_{0.5}\text{O}_2$ . *Adv Energy Mater*. 2014;4(7):1301683.
169. Ni M, Shao Z. Fuel cells that operate at 300° to 500°C. *Science*. 2020;369(6500):138-139.
170. Wu Y, Zhang J, Li L, et al. Proton conduction and fuel cell using the CuFe-Oxide mineral composite based on  $\text{CuFeO}_2$  Structure. *ACS Appl Energy Mater*. 2018;1(2):580-588.
171. Wu Y, Xia C, Zhang W, et al. Natural hematite for next-generation solid oxide fuel cells. *Adv Funct Mater*. 2016;26:938-942.
172. Zhu B, Liu X, Zhu Z, Ljungberg R. Solid oxide fuel cell (SOFC) using industrial grade mixed rare-earth oxide electrolytes. *Int J Hydrogen Energ*. 2008;33(13):3385-3392.
173. Mukundan R, Davies PK, Worrell WL. Electrochemical characterization of mixed conducting  $\text{Ba}(\text{Ce}_{0.8-y}\text{Pr}_y\text{Gd}_{0.2})\text{O}_{2.9}$  Cathodes. *J Electrochem Soc*. 2001;148(1):A82.
174. Shang M, Tong J, O'Hayre R. A promising cathode for intermediate temperature protonic ceramic fuel cells:  $\text{BaCo}_{0.4}\text{Fe}_{0.4}\text{Zr}_{0.2}\text{O}_{3-\delta}$ . *RSC Adv*. 2013;3(36):15769-15775.
175. Duan C, Tong J, Shang M, et al. Readily processed protonic ceramic fuel cells with high performance at low temperatures. *Science*. 2015;349(6254):1321-1326.
176. Ren R, Wang Z, Xu C, et al. Tuning the defects of the triple conducting oxide  $\text{BaCo}_{0.4}\text{Fe}_{0.4}\text{Zr}_{0.1}\text{Y}_{0.1}\text{O}_{3-\delta}$  perovskite toward enhanced cathode activity of protonic ceramic fuel cells. *J Mater Chem A*. 2019;7(31):18365-18372.
177. Grimaud A, Mauvy F, Bassat JM, Fourcade S, Marrony M, Grenier JC. Hydration and transport properties of the  $\text{Pr}_{2-x}\text{Sr}_x\text{NiO}_{4+\delta}$  compounds as  $\text{H}^+$ -SOFC cathodes. *J Mater Chem*. 2012;22(31):16017-16025.
178. Grimaud A, Mauvy F, Bassat JM, et al. Hydration properties and rate determining steps of the oxygen reduction reaction of perovskite-related oxides as  $\text{H}^+$ -SOFC cathodes. *J Electrochem Soc*. 2012;159(6):B683.
179. Strandbakke R, Cherepanov VA, Zuev AY, et al. Gd-and Pr-based double perovskite cobaltites as oxygen electrodes for proton ceramic fuel cells and electrolyser cells. *Solid State Ionics*. 2015;278:120-132.
180. Choi S, Yoo S, Kim J, et al. Highly efficient and robust cathode materials for low-temperature solid oxide fuel cells:  $\text{PrBa}_{0.5}\text{Sr}_{0.5}\text{Co}_{2-x}\text{Fe}_x\text{O}_{5+\delta}$ . *Sci Rep*. 2013;3:2426.
181. Yang L, Zuo C, Wang S, Cheng Z, Liu M. A novel composite cathode for low-temperature SOFCs based on oxide proton conductors. *Adv Mater*. 2008;20(17):3280-3283.
182. Yang L, Liu Z, Wang S, Choi Y, Zuo C, Liu M. A mixed proton, oxygen ion, and electron conducting cathode for SOFCs based on oxide proton conductors. *J Power Sources*. 2010;195(2):471-474.



183. Fabbri E, Bi L, Pergolesi D, Traversa E. High-performance composite cathodes with tailored mixed conductivity for intermediate temperature solid oxide fuel cells using proton conducting electrolytes. *Energy Environ Sci.* 2011;4(12):4984-4993.
184. Lee S, Park S, Wee S, Baek HW, Shin D. One-dimensional structured  $\text{La}_{0.6}\text{Sr}_{0.4}\text{Co}_{0.2}\text{Fe}_{0.8}\text{O}_{3-\delta}$ - $\text{BaCe}_{0.5}\text{Zr}_{0.35}\text{Y}_{0.15}\text{O}_{3-\delta}$  composite cathode for protonic ceramic fuel cells. *Solid State Ionics.* 2018;320:347-352.
185. Kim G, Wang S, Jacobson AJ, Reimus L, Brodersen P, Mims CA. Rapid oxygen ion diffusion and surface exchange kinetics in  $\text{PrBaCo}_2\text{O}_{5+x}$  with a perovskite related structure and ordered A cations. *J Mater Chem.* 2007;17(24):2500-2505.
186. Dong F, Ni M, Chen Y, Chen D, Tádé MO, Shao Z. Structural and oxygen-transport studies of double perovskites  $\text{PrBa}_{1-x}\text{Co}_2\text{O}_{5+\delta}$  ( $x = 0.00, 0.05, \text{ and } 0.10$ ) toward their application as superior oxygen reduction electrodes. *J Mater Chem A.* 2014;2(48):20520-20529.
187. Bu Y, Chen Y, Wei T, et al. Composites of single/double perovskites as cathodes for solid oxide fuel cells. *Energy Technol.* 2016;4(7):804-808.
188. Chen Y, Shen J, Yang G, Zhou W, Shao Z. A single-/double-perovskite composite with an overwhelming single-perovskite phase for the oxygen reduction reaction at intermediate temperatures. *J Mater Chem A.* 2017;5(47):24842-24849.
189. Bu Y, Joo S, Zhang Y, et al. A highly efficient composite cathode for proton-conducting solid oxide fuel cells. *J Power Sources.* 2020;451:227812.
190. Lee H, Lee S, Lee T, Park S, Shin D. Long term stability of porosity gradient composite cathode controlled by electro-static slurry spray deposition. *Int J Hydrogen Energ.* 2017;42(6):3748-3752.
191. Lee H, Choi J, Park I, Shin D. Electrochemical performance of continuously gradient composite cathode fabricated by electro-static slurry spray deposition. *Int J Hydrogen Energ.* 2014;39(26):14322-14327.
192. Rioja-Monllor L, Bernuy-Lopez C, Fontaine M-L, Grande T, Einarsrud M-A. Processing of high performance composite cathodes for protonic ceramic fuel cells by exsolution. *J Mater Chem A.* 2019;7(14):8609-8619.
193. Li G, Jin H, Cui Y, Gui L, He B, Zhao L. Application of a novel  $(\text{Pr}_{0.9}\text{La}_{0.1})_2(\text{Ni}_{0.74}\text{Cu}_{0.21}\text{Nb}_{0.05})\text{O}_{4+\delta}$ -infiltrated  $\text{BaZr}_{0.1}\text{Ce}_{0.7}\text{Y}_{0.2}\text{O}_{3-\delta}$  cathode for high performance protonic ceramic fuel cells. *J Power Sources.* 2017;341:192-198.
194. Song Y, Chen Y, Wang W, et al. Self-assembled triple-conducting nanocomposite as a superior protonic ceramic fuel cell cathode. *Joule.* 2019;3(11):2842-2853.
195. Tolchard J, Grande T. Physicochemical compatibility of  $\text{SrCeO}_3$  with potential SOFC cathodes. *J Solid State Chem.* 2007;180(10):2808-2815.
196. Goupil G, Delahaye T, Gauthier G, Sala B, Joud FL. Stability study of possible air electrode materials for proton conducting electrochemical cells. *Solid State Ionics.* 2012;209:36-42.
197. Lin Y, Ran R, Zheng Y, et al. Evaluation of  $\text{Ba}_{0.5}\text{Sr}_{0.5}\text{Co}_{0.8}\text{Fe}_{0.2}\text{O}_{3-\delta}$  as a potential cathode for an anode-supported proton-conducting solid-oxide fuel cell. *J Power Sources.* 2008;180(1):15-22.
198. Lin Y, Ran R, Zhang C, Cai R, Shao Z. Performance of  $\text{PrBaCo}_2\text{O}_{5+\delta}$  as a proton-conducting solid-oxide fuel cell cathode. *J Phys Chem A.* 2010;114(11):3764-3772.
199. Ding H, Xue X. Novel layered perovskite  $\text{GdBaCoFeO}_{5+\delta}$  as a potential cathode for proton-conducting solid oxide fuel cells. *Int J Hydrogen Energ.* 2010;35(9):4311-4315.
200. Zhao F, Jin C, Yang C, Wang S, Chen F. Fabrication and characterization of anode-supported micro-tubular solid oxide fuel cell based on  $\text{BaZr}_{0.1}\text{Ce}_{0.7}\text{Y}_{0.1}\text{Yb}_{0.1}\text{O}_{3-\delta}$  electrolyte. *J Power Sources.* 2011;196(2):688-691.
201. Zhao L, He B, Nian Q, et al. In situ drop-coated  $\text{BaZr}_{0.1}\text{Ce}_{0.7}\text{Y}_{0.2}\text{O}_{3-\delta}$  electrolyte-based proton-conductor solid oxide fuel cells with a novel layered  $\text{PrBaCuFeO}_{5+\delta}$  cathode. *J Power Sources.* 2009;194(1):291-294.
202. Yang Z, Ding Z, Xiao J, Zhang H, Ma G, Zhou Z. A novel cobalt-free layered perovskite-type  $\text{GdBaFeNiO}_{5+\delta}$  cathode material for proton-conducting intermediate temperature solid oxide fuel cells. *J Power Sources.* 2012;220:15-19.
203. Ding Z, Yang Z, Zhao D, Deng X, Ma G. A cobalt-free perovskite-type  $\text{La}_{0.6}\text{Sr}_{0.4}\text{Fe}_{0.9}\text{Cr}_{0.1}\text{O}_{3-\alpha}$  cathode for proton-conducting intermediate temperature solid oxide fuel cells. *J Alloy Compd.* 2013;550:204-208.
204. Zhang X, Zhou J, Wang Y. Novel layered perovskite  $\text{GdBaCuFeO}_{5+x}$  as a potential cathode for proton-conducting solid oxide fuel cells. *Ionics.* 2013;19(6):941-945.
205. Chen Y, deGlee B, Tang Y, et al. A robust fuel cell operated on nearly dry methane at 500°C enabled by synergistic thermal catalysis and electrocatalysis. *Nat Energy.* 2018;3(12):1042-1050.
206. Coors WG, Manerbino A. Characterization of composite cermet with 68 wt% NiO and  $\text{BaCe}_{0.2}\text{Zr}_{0.6}\text{Y}_{0.2}\text{O}_{3-\delta}$ . *J Membrane Sci.* 2011;376(1-2):50-55.
207. Rainwater BH, Liu M, Liu M. A more efficient anode micro-structure for SOFCs based on proton conductors. *Int J Hydrogen Energ.* 2012;37(23):18342-18348.
208. Zhang Y, Knibbe R, Sunarso J, et al. Recent progress on advanced materials for solid-oxide Fuel cells operating below 500 degrees C. *Adv Mater.* 2017;29(48):1700132.
209. Wang W, Qu J, Julião PSB, Shao Z. Recent advances in the development of anode materials for solid oxide fuel cells utilizing liquid oxygenated hydrocarbon fuels: a mini review. *Energy Technol.* 2019;7(1):33-44.
210. Yang C, Yang Z, Jin C, Xiao G, Chen F, Han M. Sulfur-tolerant redox-reversible anode material for direct hydrocarbon solid oxide fuel cells. *Adv Mater.* 2012;24(11):1439-1443.
211. Zhu T, Troiani HE, Moggi LV, Han M, Barnett SA. Ni-substituted  $\text{Sr}(\text{Ti}, \text{Fe})\text{O}_3$  SOFC anodes: achieving high performance via metal alloy nanoparticle exsolution. *Joule.* 2018;2(3):478-496.
212. Neagu D, Tsekouras G, Miller DN, Ménard H, Irvine JTS. In situ growth of nanoparticles through control of non-stoichiometry. *Nat Chem.* 2013;5(11):916-923.
213. Neagu D, Oh T-S, Miller DN, et al. Nano-socketed nickel particles with enhanced coking resistance grown in situ by redox exsolution. *Nat Commun.* 2015;6(1):1-8.
214. Liu S, Liu Q, Fu X-Z, Luo J-L. Cogeneration of ethylene and energy in protonic fuel cell with an efficient and stable anode anchored with in-situ exsolved functional metal nanoparticles. *Appl Catal B-Environ.* 2018;220:283-289.
215. Duan C, Kee RJ, Zhu H, et al. Highly durable, coking and sulfur tolerant, fuel-flexible protonic ceramic fuel cells. *Nature.* 2018;557(7704):217-222.
216. Liu Z, Zhou M, Chen M, et al. A high-performance intermediate-to-low temperature protonic ceramic fuel cell with in-situ exsolved nickel nanoparticles in the anode. *Ceram Int.* 2020;46(12):19952-19959.
217. Liu S, Chuang KT, Luo J-L. Double-layered perovskite anode with in situ exsolution of a Co-Fe alloy to cogenerate ethylene



- and electricity in a proton-conducting ethane fuel cell. *ACS Catal.* 2016;6(2):760-768.
218. Ricote S, Bonanos N, Manerbino A, Coors WG. Conductivity study of dense  $\text{BaCe}_x\text{Zr}_{(0.9-x)}\text{Y}_{0.1}\text{O}_{(3-\delta)}$  prepared by solid state reactive sintering at 1500°C. *Int J Hydrogen Energ.* 2012;37(9):7954-7961.
219. Shimada H, Li X, Hagiwara A, Ihara M. Proton-conducting solid oxide fuel cells with yttrium-doped barium zirconate for direct methane operation. *J Electrochem Soc.* 2013;160(6):F597.
220. Fabbri E, Pergolesi D, D'Epifanio A, et al. Improving the performance of high temperature protonic conductor (HTPC) electrolytes for solid oxide fuel cell (SOFC) applications. *Trans Tech Publ.* 2010;336-339.
221. Sawant P, Varma S, Wani BN, Bharadwaj SR. Synthesis, stability and conductivity of  $\text{BaCe}_{0.8-x}\text{Zr}_x\text{Y}_{0.2}\text{O}_{3-\delta}$  as electrolyte for proton conducting SOFC. *Int J Hydrogen Energ.* 2012;37(4):3848-3856.
222. Yoo C-Y, Yun DS, Joo JH, Yu JH. The effects of NiO addition on the structure and transport properties of proton conducting  $\text{BaZr}_{0.8}\text{Y}_{0.2}\text{O}_{3-\delta}$ . *J Alloy Compd.* 2015;621:263-267.
223. Babilo P, Uda T, Haile SM. Processing of yttrium-doped barium zirconate for high proton conductivity. *J Mater Res.* 2007;22(5):1322-1330.
224. Yamazaki Y, Hernandez-Sanchez R, Haile SM. High total proton conductivity in large-grained yttrium-doped barium zirconate. *Chem Mater.* 2009;21(13):2755-2762.
225. Cervera RB, Oyama Y, Miyoshi S, Kobayashi K, Yagi T, Yamaguchi S. Structural study and proton transport of bulk nanograined Y-doped  $\text{BaZrO}_3$  oxide protonics materials. *Solid State Ionics.* 2008;179(7-8):236-242.
226. Taillades G, Dailly J, Taillades-Jacquín M, et al. Intermediate temperature anode-supported fuel cell based on  $\text{BaCe}_{0.9}\text{Y}_{0.1}\text{O}_3$  electrolyte with novel  $\text{Pr}_2\text{NiO}_4$  cathode. *Fuel Cells.* 2010;10(1):166-173.
227. Pergolesi D, Fabbri E, Traversa E. Chemically stable anode-supported solid oxide fuel cells based on Y-doped barium zirconate thin films having improved performance. *Electrochem Commun.* 2010;12(7):977-980.
228. Sun W, Yan L, Shi Z, Zhu Z, Liu W. Fabrication and performance of a proton-conducting solid oxide fuel cell based on a thin  $\text{BaZr}_{0.8}\text{Y}_{0.2}\text{O}_{3-\delta}$  electrolyte membrane. *J Power Sources.* 2010;95(15):4727-4730.
229. Xiao J, Sun W, Zhu Z, Tao Z, Liu W. Fabrication and characterization of anode-supported dense  $\text{BaZr}_{0.8}\text{Y}_{0.2}\text{O}_{3-\delta}$  electrolyte membranes by a dip-coating process. *Mater Lett.* 2012;73:198-201.
230. Sun W, Liu M, Liu W. Chemically stable yttrium and tin co-doped barium zirconate electrolyte for next generation high performance proton-conducting solid oxide fuel cells. *Adv Energ Mater.* 2013;3(8):1041-1050.
231. Hanifi AR, Sandhu NK, Etsell TH, Luo J-L, Sarkar P. Fabrication and characterization of a tubular ceramic fuel cell based on  $\text{BaZr}_{0.1}\text{Ce}_{0.7}\text{Y}_{0.1}\text{Yb}_{0.1}\text{O}_{3-\delta}$  proton conducting electrolyte. *J Power Sources.* 2017;341:264-269.

**How to cite this article:** Zhang W, Hu YH. Progress in proton-conducting oxides as electrolytes for low-temperature solid oxide fuel cells: From materials to devices. *Energy Sci Eng.* 2021;00:1–28. <https://doi.org/10.1002/ese3.886>